

AD-A154 122

FUNDAMENTAL STUDIES OF BETA PHASE DECOMPOSITION MODES
IN TITANIUM ALLOYS. (U) CARNEGIE MELLON UNIV PITTSBURGH
PA DEPT OF METALLURGICAL ENGI. H I AARONSON ET AL.

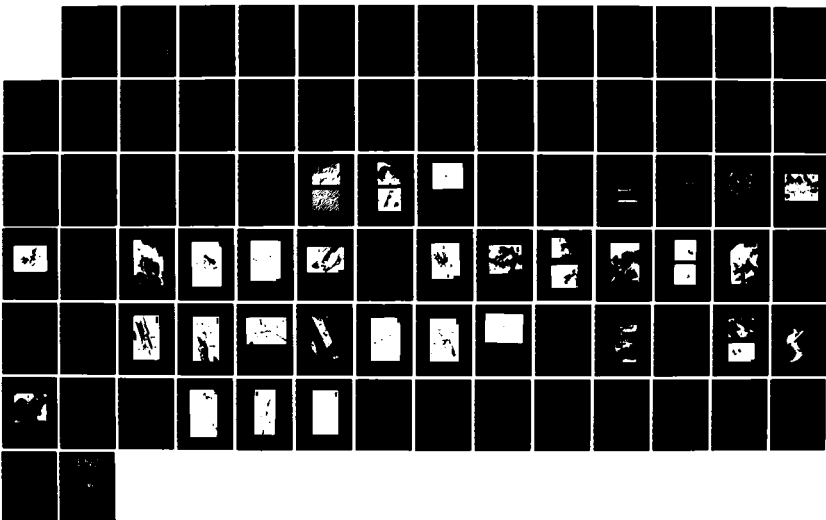
1/1

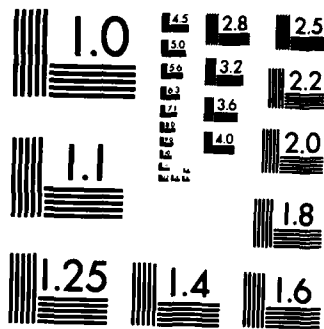
UNCLASSIFIED

24 JAN 85 AFOSR-TR-85-0393 AFOSR-80-0021

F/G 11/6

NL





MICROCOPY RESOLUTION TEST CHART
NATIONAL BUREAU OF STANDARDS-1963-A

AFOSR-TR. 85-0393

(2)

AD-A154 122

~~Interim~~ ^{Final} Technical Report

from

Department of Metallurgical Engineering
and Materials Science
Carnegie-Mellon University

to

Air Force Office of Scientific Research
Electronic and Solid State Sciences
Bolling Air Force Base
Washington, DC 20332

on

Fundamental Studies of Beta Phase Decomposition Modes
in Titanium Alloys

H.I. Aaronson, Principal Investigator
A.M. Dalley, Graduate Student
H.J. Lee, Graduate Student
E.S.K. Menon, Graduate Student

for the period

1 October 1983 - 30 September 1984

AFOSR-80-0021

January 24, 1985

DTIC
ELECTE
MAY 24 1985
B

DTIC FILE COPY

Approved for public release;
distribution unlimited.

85 423 004

UNCLASSIFIED

SECURITY CLASSIFICATION OF THIS PAGE

AD A154122

REPORT DOCUMENTATION PAGE

1a. REPORT SECURITY CLASSIFICATION UNCLASSIFIED			1b. RESTRICTIVE MARKINGS		
2a. SECURITY CLASSIFICATION AUTHORITY			3. DISTRIBUTION/AVAILABILITY OF REPORT Approved for public release; distribution unlimited.		
2b. DECLASSIFICATION/DOWNGRADING SCHEDULE					
4. PERFORMING ORGANIZATION REPORT NUMBER(S)			5. MONITORING ORGANIZATION REPORT NUMBER(S) AFOSR-TR- 85-0393		
6a. NAME OF PERFORMING ORGANIZATION Carnegie-Mellon University		6b. OFFICE SYMBOL (If applicable)	7a. NAME OF MONITORING ORGANIZATION Air Force Office of Scientific Research		
6c. ADDRESS (City, State and ZIP Code) 5000 Forbes Avenue Pittsburgh, PA. 15213			7b. ADDRESS (City, State and ZIP Code) Bldg 410 Bolling AFB DC 20332-6448		
8a. NAME OF FUNDING/SPONSORING ORGANIZATION AFOSR		8b. OFFICE SYMBOL (If applicable) NE	9. PROCUREMENT INSTRUMENT IDENTIFICATION NUMBER AFOSR-YO-0021		
8c. ADDRESS (City, State and ZIP Code) Bolling AFB DC 20332-6448			10. SOURCE OF FUNDING NOS.		
			PROGRAM ELEMENT NO. 61102F	PROJECT NO. 2306	TASK NO. A1
			WORK UNIT NO.		
11. TITLE (Include Security Classification) Fundamental Studies of Beta Phase Decomposition Modes in Titanium Alloys					
12. PERSONAL AUTHOR(S) E. I. Aaronson, A. M. Dalley, H. J. Lee and E. S. K. Menon					
13a. TYPE OF REPORT Final		13b. TIME COVERED FROM 1/10/83 TO 30/9/84		14. DATE OF REPORT (Yr., Mo., Day) 1985, Jan. 24	
				15. PAGE COUNT 27	
16. SUPPLEMENTARY NOTATION Final Beta yields Alpha SubD					
17. COSATI CODES			18. SUBJECT TERMS (Continue on reverse if necessary and identify by block number)		
FIELD	GROUP	SUB. GR.	Alpha		
19. ABSTRACT (Continue on reverse if necessary and identify by block number) Kinetics of $\beta \rightarrow \alpha$ massive transformation were compared with those of grain boundary proeutectoid α precipitation in Ti-Ag and Ti-Co alloys, using measured or calculated nucleation and growth kinetics data and Cahn analysis of overall transformation kinetics of grain boundary nucleated reactions, successfully explained presence of massive transformation only in Ti-Ag and α allotriomorphs only in Ti-Co. New explanation developed, on thermodynamic grounds, for replacement of "normal" proeutectoid α plates with well-formed "black plates" α + lower reaction temperatures. Bainite nodules in hypereutectoid Ti-Cr and in hypoeutectoid Ti-Co and Ti-Fe were found to exhibit misfit dislocation and ledge structures. Nodules in Ti-Cr grew at approximately volume diffusion-controlled rates; but reanalysis is now needed in terms of ledge mechanism. Eutectoid α often found to differ slightly in orientation from adjacent proeutectoid α plates.					
20. DISTRIBUTION/AVAILABILITY OF ABSTRACT UNCLASSIFIED/UNLIMITED <input checked="" type="checkbox"/> SAME AS RPT. <input type="checkbox"/> DTIC USERS <input type="checkbox"/>			21. ABSTRACT SECURITY CLASSIFICATION UNCLASSIFIED		
22a. NAME OF RESPONSIBLE INDIVIDUAL DR. IVAN Caplan			22b. TELEPHONE NUMBER (Include Area Code) (202) 767-4933		22c. OFFICE SYMBOL NE

DD FORM 1473, 83 APR

EDITION OF 1 JAN 73 IS OBSOLETE.

UNCLASSIFIED

SECURITY CLASSIFICATION OF THIS PAGE

Fundamental Studies of Beta Phase Decomposition Modes
in Titanium Alloys

H.I. Aaronson, A.M. Dalley, H.J. Lee and E.S.K. Menon

Abstract

These studies on diffusional phase transformations in titanium and related alloy systems are intended to develop further the scientific base needed to design alloys based upon these transformations which may exhibit significantly improved combinations of mechanical properties. During the past grant year, using appropriate modifications of Cahn's analysis of the overall transformation kinetics of grain boundary nucleated reactions, the kinetics of the $\beta \rightarrow \alpha_m$ massive transformation were compared with those of grain boundary allotriomorphs of proeutectoid alpha in (representative) Ti-Ag and Ti-Co alloys. Predominance of the massive transformation in Ti-Ag and of the proeutectoid alpha reaction in Ti-Co was successfully explained using both experimental and estimated data on nucleation and growth kinetics of both types of transformation. A new explanation has been developed and partially validated for the "black plate" phenomenon, wherein thin, well-formed, fast growing alpha plates replace normal degenerate alpha plates at lower temperatures in Ti-Cr and other Ti-X systems. This replacement was deduced to arise as a consequence of positive deviations of the beta matrix from ideality; this thermodynamic factor generates a metastable equilibrium monotectoid reaction whose $\beta / (\alpha + \beta_1)$ boundaries terminate at the spinodal compositions. Below a critical temperature, equilibrium with only the Cr-rich boundary is feasible, leading to a drastic change in composition of the beta in contact with alpha plates. This change is predicted to yield a much lower density of growth ledges. A detailed study of bainite nodule formation in a hyper-eutectoid Ti-25% Cr alloy showed extensive evidence of faceting at both beta:bainitic alpha and beta:bainitic TiCr_2 boundaries. Unlike pearlite, TiCr_2 crystals in a given nodule do not have a single orientation relationship. The growth kinetics

1



A-1



des
12

-2-

of bainite nodules are approximately those permitted by volume interdiffusion through the beta matrix. Proeutectoid alpha and bainite structures examined in hypoeutectoid Ti-Co and Ti-Fe alloys also show extensive evidence of misfit dislocations and growth ledges on proeutectoid alpha, eutectoid alpha generated during the bainite reaction and on the beta:compound and alpha:compound boundaries, though detailed sorting out of these features remains to be accomplished. It has thus become evident that operation of the ledge mechanism during bainite growth is general and that kinetic theory will have to be revised accordingly. Eutectoid alpha was often found to have a slightly different orientation relationship with respect to beta than the proeutectoid alpha against which it formed.

I. Introduction

This program is primarily concerned with fundamental studies of the crystallography, morphology, kinetics and mechanisms of the proeutectoid alpha and the bainite reactions in Ti-X alloys. Active interest continues, though, in the massive transformation, particularly in Ti-X alloys but also in a more general sense, with the ultimate goal of understanding why this transformation predominates in only three Ti-X eutectoid systems while the proeutectoid alpha (and its derivative, the bainite) reaction are the only transformation mechanisms operative at higher reaction temperatures in at least ten other Ti-X eutectoid systems.

By the term "bainite" we mean the product of a non-lamellar, i.e., a non-cooperative or non-pearlitic mode of eutectoid decomposition (1,2). Critical consideration of the more generally accepted definition of bainite, as precipitate plate growth by a diffusion-controlled shear mechanism does, however, play a role in our bainite program.

II. The Proeutectoid Alpha Reaction

This program constitutes the Ph.D. Thesis research of Mr. E. Sarath Kumar Menon (except for subsection II-E)

A. Introduction

Attention has been focussed this year upon one of the original objectives of this program, namely, an evaluation of the conditions under which the massive and the proeutectoid alpha transformations predominate over one another. Because more than 14 Ti-X eutectoid systems have been identified, with the $\beta \rightarrow \alpha_m$ massive transformation occurring when X is Ag (3), Au (3), In (4) and Si (3) and the proeutectoid alpha reaction being the principal initial decomposition mode when X is Bi, Co, Cr, Cu, Fe, Mn, Ni, Pb, Pd and Pt (5,6), the Ti-X eutectoid systems provide en bloc an ideal "test vehicle" for such an analysis.

During the previous grant year, we showed that under nearly all circumstances, the nucleus of the massive transformation has the same composition as that of the proeutectoid alpha reaction (7). Hence evaluation of the kinetic competition between the proeutectoid alpha and the massive alpha transformations requires primarily that the growth kinetics of alpha during the two reactions be compared. This has been done for the $\beta \rightarrow \alpha_m$ reaction and the $\beta \rightarrow \alpha + \beta_1$ reaction (where β_1 denotes compositionally enriched β) in Ti-Ag and Ti-Co alloys. These transformations were used because of the extensive documentation available upon them.

B. Growth Kinetics

The $\alpha + \beta$ regions of the Ti-Ag and the Ti-Co systems, showing the metastable extensions of the phase boundaries and the T_0 curves calculated from the optimized phase diagrams (8,9), are presented in Fig.1. It is immediately apparent that the Ti-Ag system is characterized by a narrow and nearly horizontal $\alpha + \beta$ region, whereas the Ti-Co system has a wider, more nearly vertical $\alpha + \beta$ region. Ti-Au and Ti-Si have an $\alpha + \beta$ region similar to that of Ti-Ag while this region in Ti-Co is representative of that in many other Ti-X eutectoid systems. These differences in

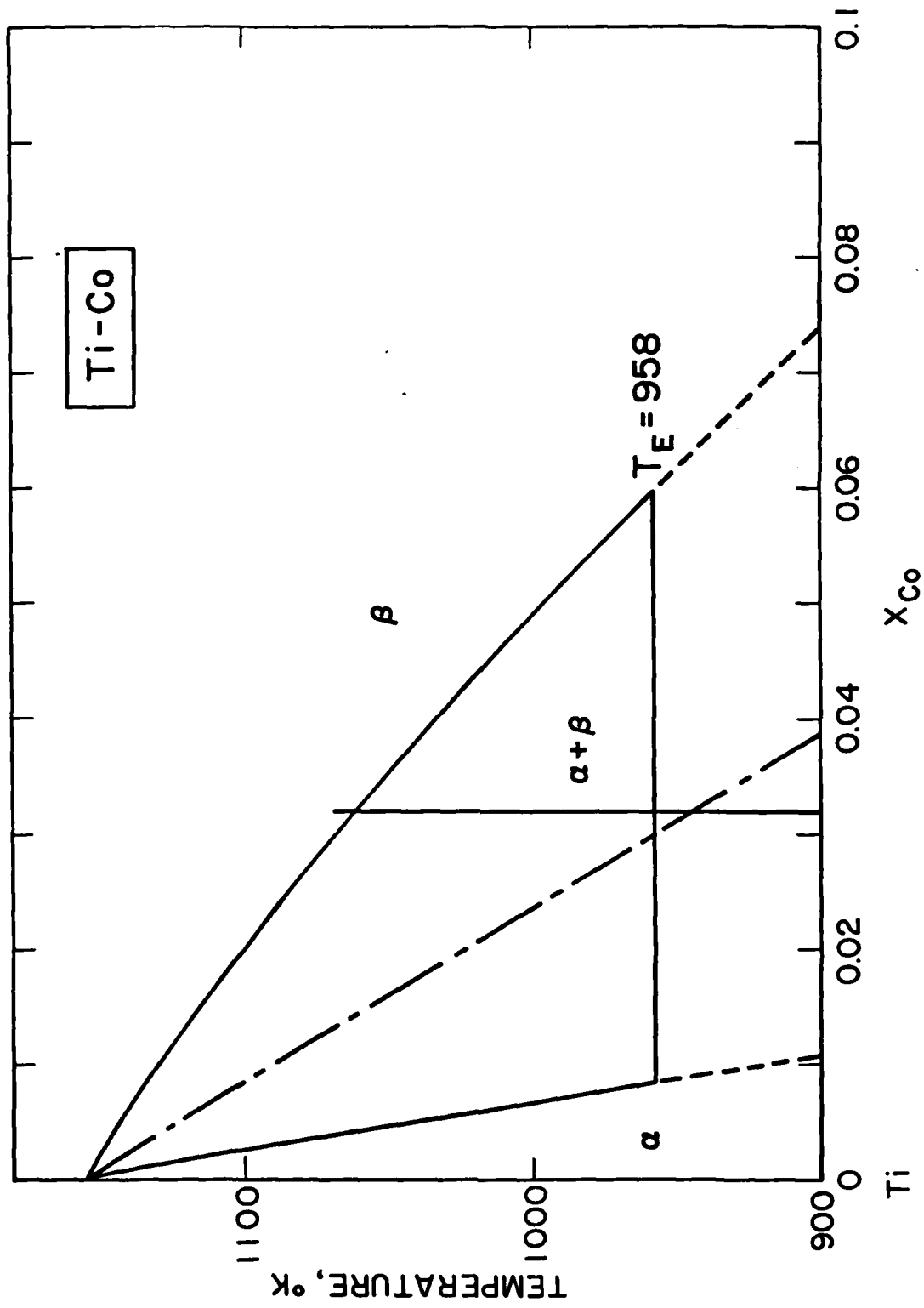


Fig. 1(a)

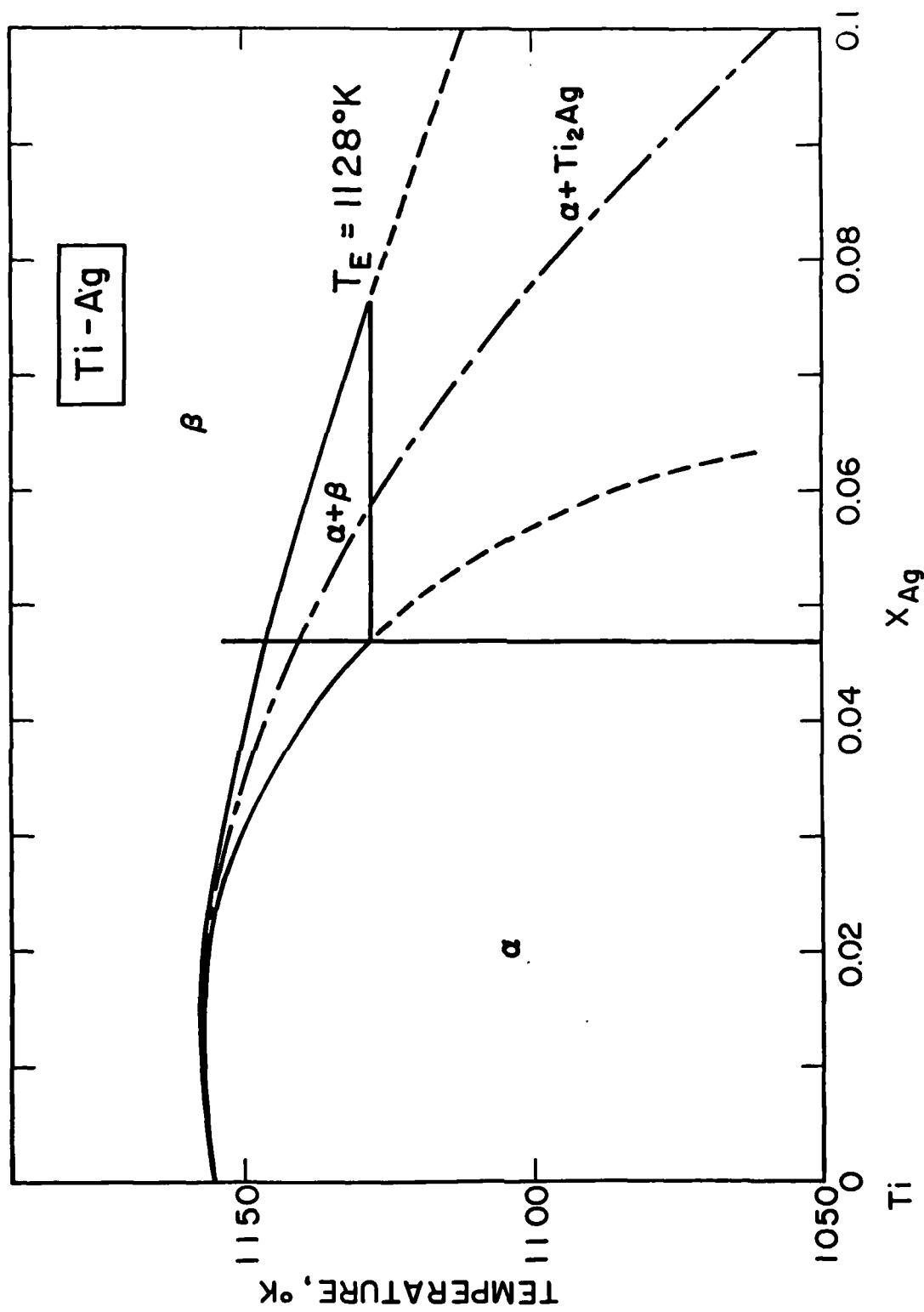


Fig. 1(b)

Fig. 1 : Ti-rich end of the (a) Ti-Co and (b) Ti-Ag phase diagrams. The phase boundaries were calculated from the thermodynamic parameters reported in refs. 38 and 39. The metastable phase boundaries are shown in dashed lines and the T_o - X curves are drawn in dash-dot lines.

phase diagram geometry markedly affect the variation with temperature of the chemical free energy change driving growth of α_m . Fig. 2 illustrates the thermodynamic driving force associated with the two modes of transformation. Alloy X_1 can undergo a massive transformation and can be termed non-competitive (10) while the $\beta \rightarrow \alpha_m$ reaction in alloy X_2 is subject to suppression by the $\beta \rightarrow \alpha + \gamma$ reaction which has a higher driving force for growth, $\Delta G^{\beta \rightarrow \alpha + \gamma}_m$ as indicated in Fig. 2.

The quantities $\Delta G^{\beta \rightarrow \alpha}$ and $\Delta G^{\beta \rightarrow \alpha + \beta_1}$ were evaluated as follows. The first one is simply computed as:

$$\Delta G^{\beta \rightarrow \alpha} = G^\alpha(x) - G^\beta(x) \quad [1]$$

where G^α and G^β represent the molar free energies of the α and the β phases and x is the composition. These free energies have been evaluated as (8,9):

Ti-Ag system:

$$G^{\alpha, \text{excess}} = x(1-x) \{26000 - 60T - 9000(1-2x)\} \quad [2]$$

$$G^{\beta, \text{excess}} = x(1-x) \{-9000 - 60T - 9000(1-2x)\}$$

Ti-Ag system:

$$G^{\alpha, \text{excess}} = x(1-x) \{47900 - 25000(1-2x)\} \quad [3]$$

$$G^{\beta, \text{excess}} = 24432 x(1-x)$$

The driving force, $\Delta G^{\beta \rightarrow \alpha + \beta_1}$, for the precipitation reaction is obtained from the relationship:

$$\Delta G^{\beta \rightarrow \alpha + \beta_1} = [(1-x) \bar{G}_A^\alpha + x \bar{G}_B^\alpha] - G^\beta \quad [4]$$

where \bar{G}_A and \bar{G}_B represent the partial molar free energies of titanium (A) and the solute (B) in the α phase, respectively. The driving force for the two reactions, viz., massive transformation and precipitation reaction, were calculated for representative alloys in both Ti-Co and Ti-Ag, with results as shown in Fig. 3. From this figure it can be seen that even though the driving force for the precipitation reaction is always higher in both alloys chosen in the Ti-Ag case, at temperatures not far below the T_0 temperature, the driving force for the massive reaction becomes comparable to that for the precipitation reaction.

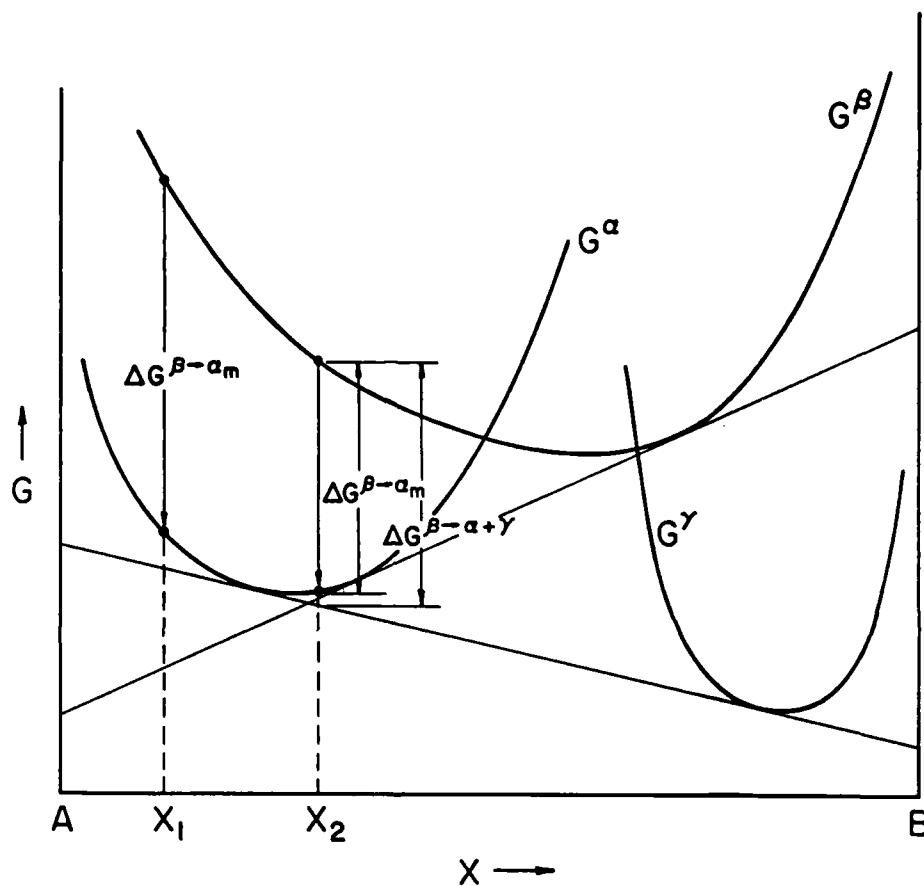


Fig. 2 : Schematic free energy-composition diagram showing the driving force for massive growth, $\Delta G^{\beta \rightarrow \alpha_m}$, in a binary alloy system.

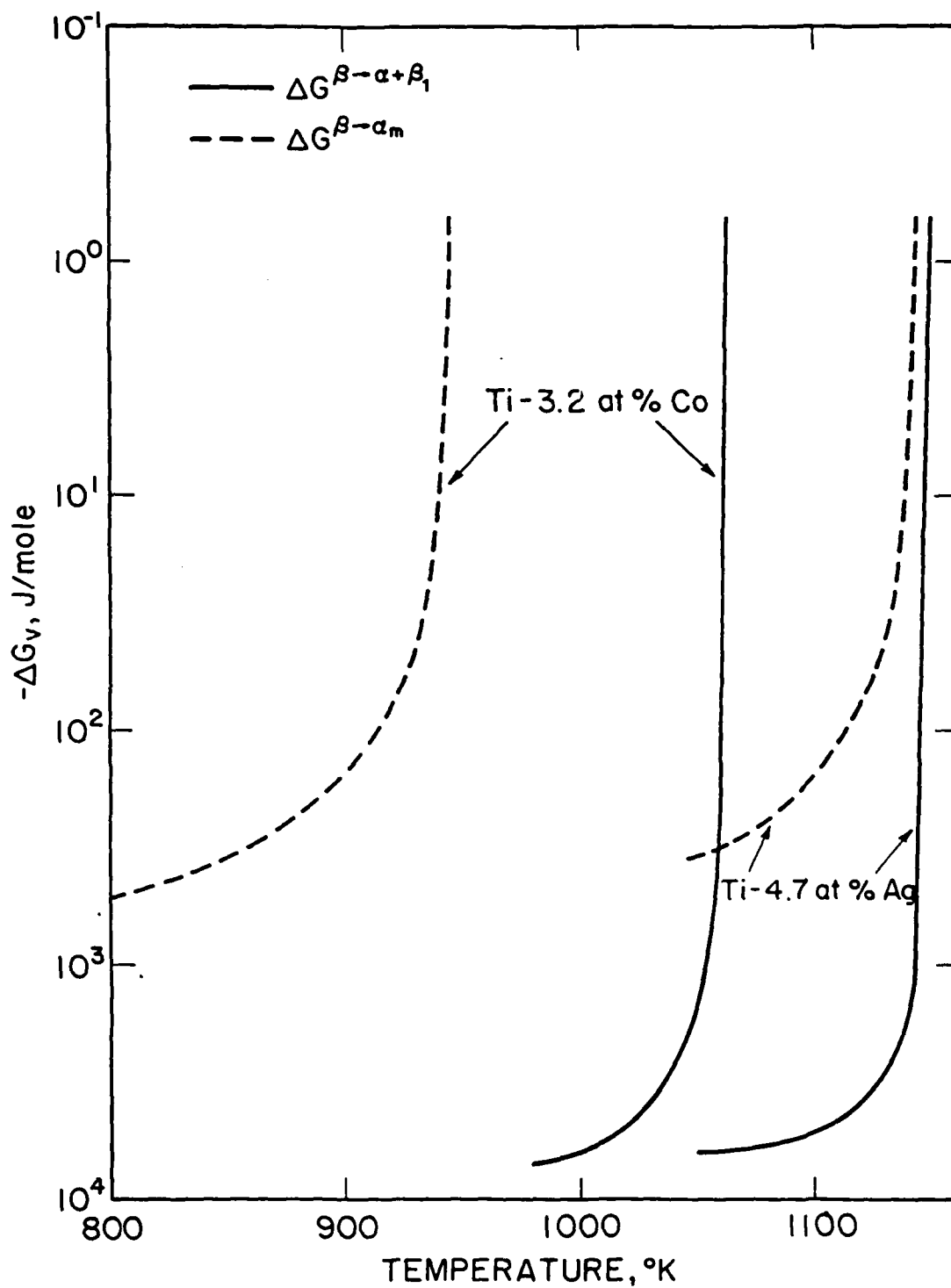


Fig. 3 : $\Delta G^{\beta \rightarrow \alpha_m}$, the driving force for massive growth and $\Delta G^{\beta \rightarrow \alpha + \beta_1}$, the driving force for equilibrium α precipitation vs isothermal reaction temperature for Ti-3.2 at% Co and Ti-4.7 at% Ag.

The massive growth rate, V , is calculated from the equation derived for the growth process controlled by the thermally activated atomic jumping across the interface (112), viz:

$$V = \frac{\delta kT}{h} \left(- \frac{\Delta G^{\beta \rightarrow \alpha}_m}{RT} \right) \exp \left(- \frac{\Delta G_{D_b}}{RT} \right) \quad [5]$$

where k = Boltzmann's Constant, h = Planck's constant, R = gas constant, T = temperature, δ = interface thickness and ΔG_{D_b} = activation free energy for trans-interface boundary diffusion. An estimate of ΔG_{D_b} was obtained using the grain boundary diffusion constant correlation reported by Brown and Ashby (12) for bcc transition metals, viz:

$$\delta D_b = 3.4 \times 10^{-13} \cdot \exp(-11.7 \frac{T_m}{T} \cdot C) \text{ m}^2/\text{s} \quad [6]$$

Here the temperatures are in °K. A rough estimate of the parameter C appearing in equation [6] using the values from ref. (12), shows that it is approximately equal to unity. The activation entropy component of ΔG_{D_b} was assigned the conventionally used value of $3R$.

The growth rate of the precipitate phase in the $\beta \rightarrow \alpha + \beta_1$ reaction was calculated using the analysis for volume diffusion controlled growth of ellipsoidal precipitates developed by Horvay and Cahn (13). Assuming that the grain boundary allotriomorphs of the α phase can be modelled as oblate ellipsoids of revolution, the parabolic growth rate constant, α_p , is obtained from the relation (14):

$$\alpha_p = 2(\Omega D_v)^{1/2} \quad [7]$$

where D_v is the volume diffusivity and Ω is the solution to the transcendental equation:

$$2e^{\Omega} \Omega^{3/2} \left\{ \frac{e^{-\Omega}}{\Omega^{1/2}} - \pi^{1/2} \operatorname{erfc}(\Omega^{1/2}) \right\} = \frac{x_{\beta}^{\beta\alpha} - x_{\beta}}{x_{\beta}^{\beta\alpha} - x_{\alpha}^{\alpha\beta}} \quad [8]$$

where x_{β} is the alloy composition and $x_{\beta}^{\beta\alpha}$ and $x_{\alpha}^{\alpha\beta}$ correspond to the phase boundary compositions at the reaction temperature. The volume diffusivities of the solutes are:

β Ti-Co (15):

$$D = 130 \times 10^{-4} \exp \left(\frac{-30900}{RT} \right) \text{ cm}^2/\text{sec} \quad [9]$$

β Ti-Ag (16):

$$D = 30 \times 10^{-4} \exp \left(\frac{-43000}{RT} \right) \text{ cm}^2/\text{sec} \quad [10]$$

The growth rate constants calculated from eqns. [5], [7] and [8] for two sample alloys are shown in Fig. 4. From this figure, it can be seen that in the Ti-Co alloy (Fig. 4a), the precipitation reaction is the only possible reaction over a wide temperature range while in the Ti-Ag alloy (Fig. 4b), this situation is observed over only a very narrow temperature region. Otherwise, the growth kinetics of massive alpha are orders of magnitude faster than those of proeutectoid alpha at nearly all temperatures (and at a reaction time of, say, one sec.) where the massive transformation is thermodynamically feasible. These results make clear that given equal nucleation rates, the choice of the transformation process is determined by growth kinetics and that the relative values of the two sets of kinetics are dictated by the temperature difference between the transus, T_{β}^{α} , and T_o . A small value of this term allows the massive transformation to develop while precipitation kinetics are still slow; quenching past the precipitation-only region is thus readily accomplished. In the reverse situation, precipitation predominates.

C. Overall Transformation Kinetics

The overall transformation kinetics of grain boundary nucleated reactions are conveniently studied by applying an analysis developed by Cahn (17) for the linear growth of spherical precipitates. The fraction of the β matrix transformed to α_m , denoted by f_m , is expressed by:

$$f_m = 1 - \exp [-b^{-1/3} f(a)] \quad [11]$$

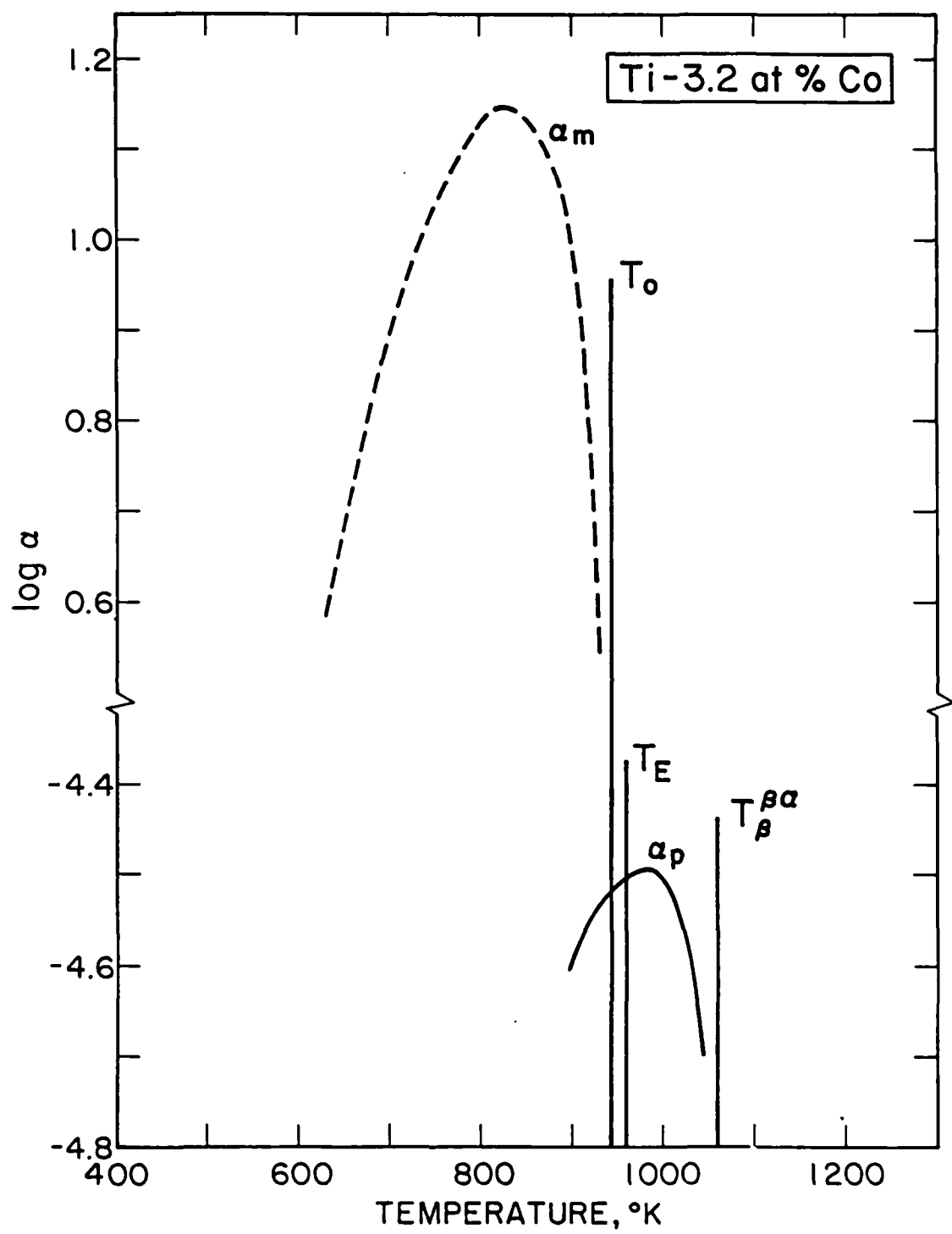


Fig. 4(a)

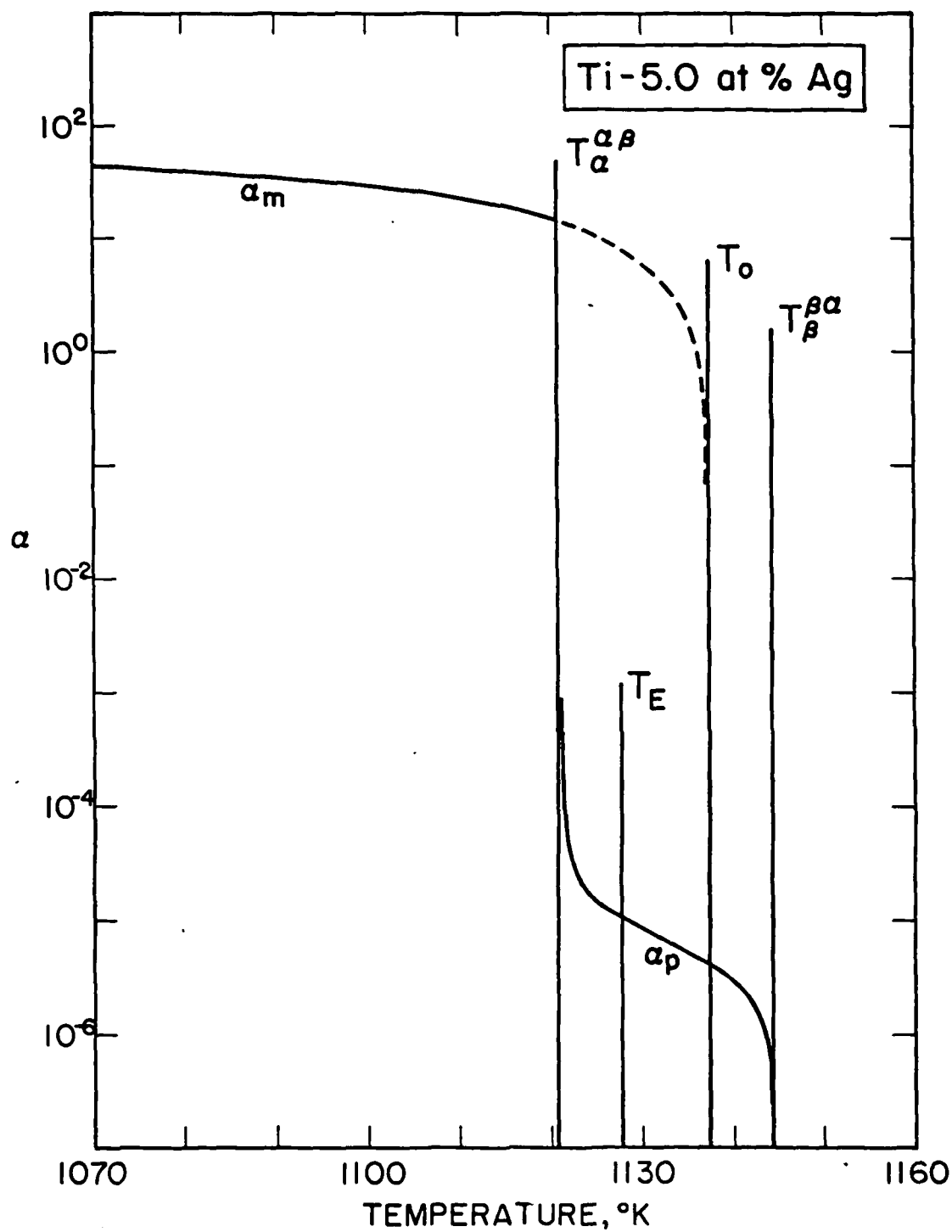


Fig. 4(b)

Fig. 4 : Calculated parabolic rate constant, α , and the massive growth rate, α_m , for (a) Ti-3.2 at% Co and (b) Ti-5.0 at% Ag. The T_0 and the β -transus temperatures are also indicated.

where:

$$a = (J^* V^2)^{1/3} t \quad [12]$$

$$b = \frac{J^*}{8VS} \quad [13]$$

and:

$$f(a) = a \int_0^1 \left\{ 1 - \exp\left[-\pi a^3 \left(\frac{2}{3} m^3 - m^2 - \frac{1}{3}\right)\right] \right\} dm \quad [14]$$

$$m = y/vt$$

Here, S is the grain boundary area per unit volume, t is the isothermal reaction time and y is the perpendicular distance between the grain boundary plane and the plane of polish. The fraction, f_p , β matrix transformed to grain boundary allotromorphs can be expressed in a similar fashion (18) by modelling these precipitates as oblate ellipsoids growing with parabolic rather than linear kinetics. The resulting equations are (18):

$$f_p = 1 - \exp - b^{-1/2} f(a) \quad [15]$$

where:

$$a = \left(\frac{J_s^* \alpha^2}{R^2} \right)^{1/2} t \quad [16]$$

$$b = \frac{J_s^* t}{4R^2 S^2} \quad [16]$$

and:

$$f(a) = a \int_0^1 \left\{ 1 - \exp\left[-\pi a^2 \left(\frac{1}{2} - m^2 + \frac{1}{2} m^4\right)\right] \right\} dm \quad [17]$$

$$m = y/\alpha_p \cdot t^{1/2} \quad [18]$$

Representative volume fraction versus time plots obtained by using these equations for the Ti-Co and Ti-Ag alloys are shown in Fig. 5. It can be seen that in the case of the Ti-Co alloy (Fig.5a), f_p increases more rapidly than f_m , whereas the reverse situation is observed in the case of the Ti-Ag alloy. From plots similar to those shown in Fig. 5, we can construct the TTT diagram for each mode of growth,

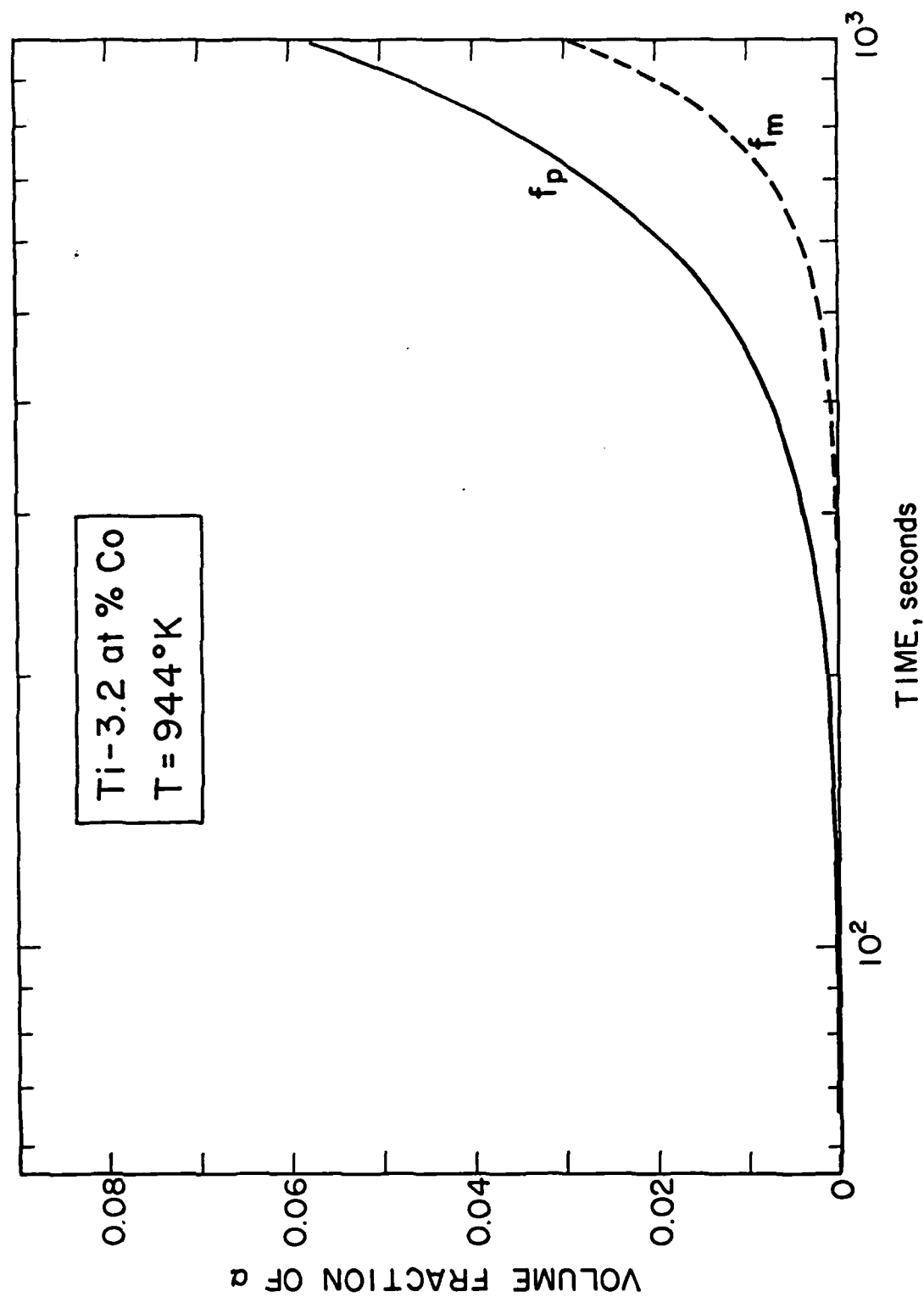


Fig. 5(a)

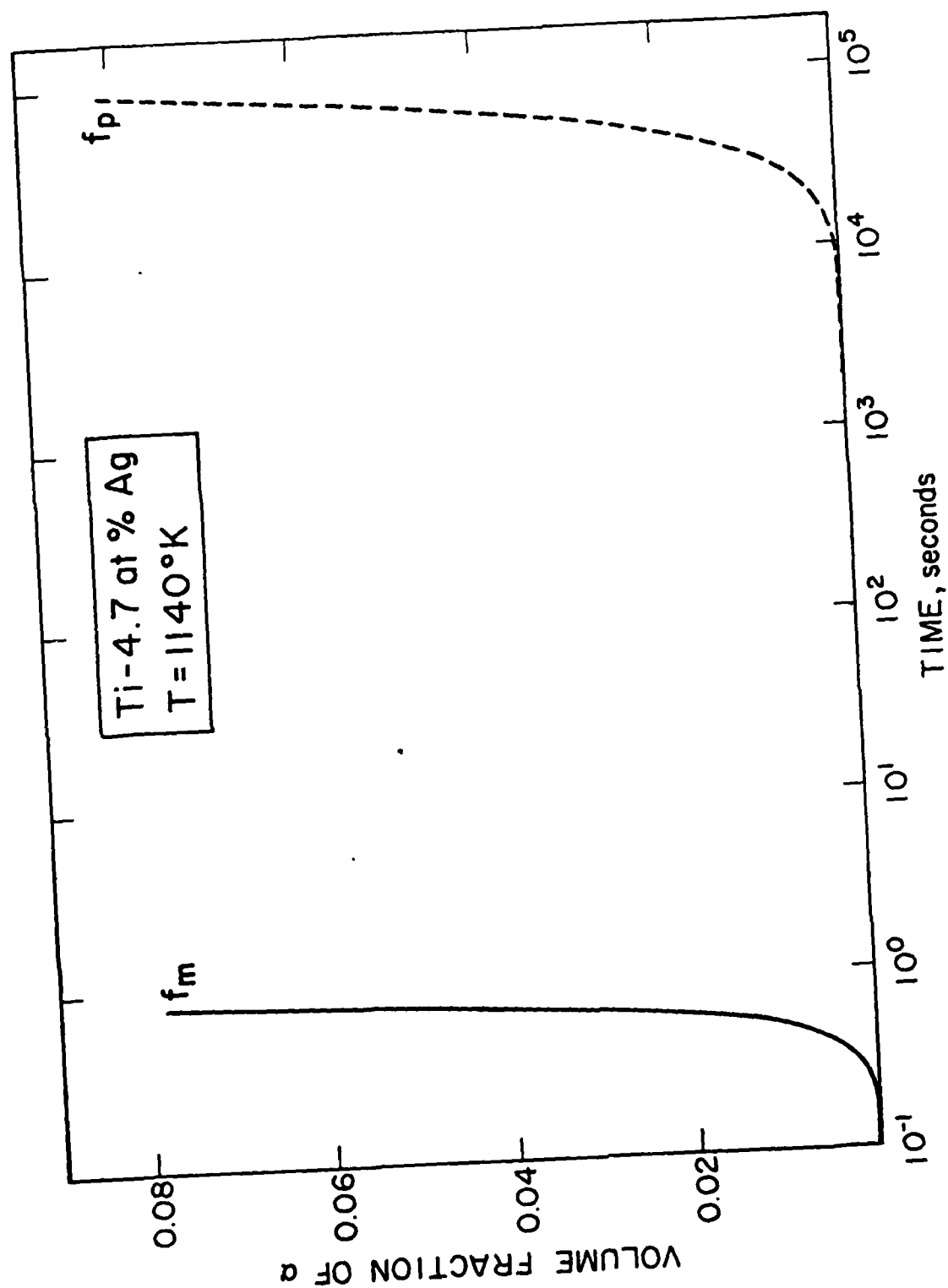


Fig. 5(b)

Fig. 5: Calculated volume fraction vs time plots. f and f_m are the volume fractions expected by equilibrium precipitation and by massive transformation respectively. Results for (a) Ti-3.2 at% Co and (b) Ti-4.7 at% Ag. The curves corresponding to the experimentally observed reaction modes are drawn as continuous lines.

as shown in Fig. 6. In these plots, the time required for the initiation of the $\beta \rightarrow \alpha_m$ and the $\beta \rightarrow \alpha + \beta_1$ reactions, taken as the time needed to obtain a volume fraction of 1%, is plotted as a function of temperature. The transformation mode which predominates and thus the one that is observed is the one whose TTT-start curve lies at the shorter times. In Fig. 6b in which the TTT curves for the Ti-Ag alloy are presented, it is very clear that the massive transformation predominates over the equilibrium reaction at all temperatures, even above the eutectoid temperature. However, Fig. 6a shows that while the equilibrium precipitation reaction is preferred above and somewhat below the eutectoid temperature, the massive transformation is preferred at lower temperatures. However, the M_s temperature of the Ti-Co alloy (19), falling at ~ 850 K, indicates that much of the predicted region of the massive transformation will be pre-empted by martensite formation.

D. Mechanism of "Black Plate" Formation

"Black plates" were first reported in a hypoeutectoid Ti-Cr in 1957; initial observations on them were made solely by optical microscopy(5). As part of the present program, they have been further investigated with both optical, and especially, transmission electron microscopy, and a model for their origin has been developed. Black plates are distinguished from normal Widmanstätten α plates by the following characteristics:

(a) Very thin, well formed black plates precipitate at lower reaction temperatures and replace the degenerate normal proeutectoid α plates which form at higher isothermal reaction temperatures. (This observation was first reported in ref.(5); all succeeding results were obtained during the present investigation);

(b) SAD pattern analysis showed that both types of α plates are h.c.p. and obey the Burgers orientation relationship with respect to the matrix β phase;

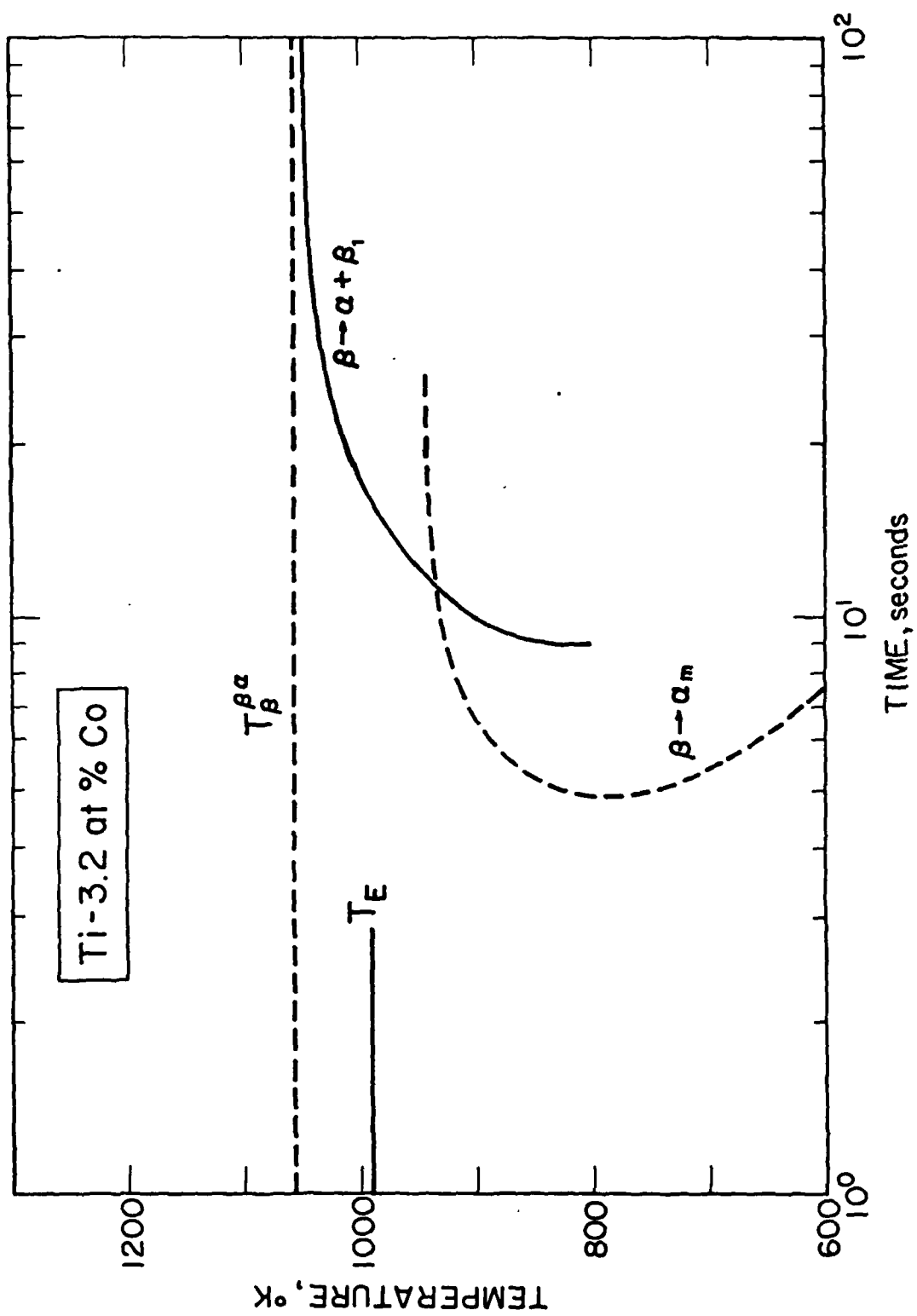


Fig. 6(a)

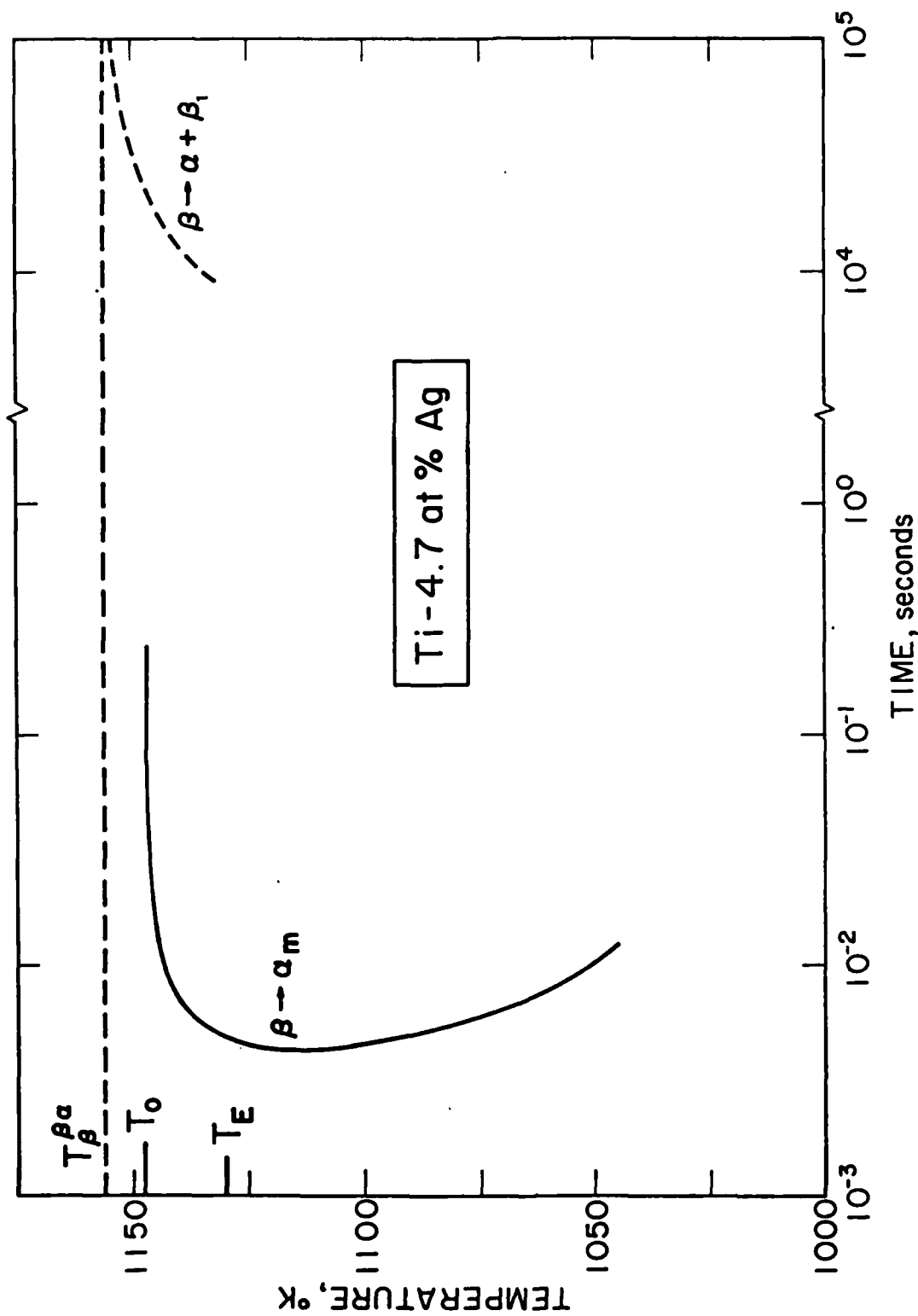


Fig. 6(b)

Fig. 6 : Calculated TTT curves for the $\beta \rightarrow \alpha + \beta_1$ and the $\beta \rightarrow \alpha_m$ reactions in (a) Ti-3.2 at% Co and (b) Ti-4.7 at% Ag. The TTT curves were calculated for a volume fraction of 0.01. Notice that the TTT curve for the precipitation reaction in Ti-3.2 at% Co lies to the left of that for the massive reaction while the reverse is true for the Ti-4.7 at% Ag alloy, again conforming to the experimental observations.

(c) The black plates are associated with a $\{110\}_\beta$ habit in contrast to the near- $\{111\}_\beta$ habit that is usually exhibited by normal α plates in Ti alloys (20,21).

(d) The lengthening kinetics of black plates are significantly higher than that of normal α plates at a given reaction temperature;

(e) Black plates appear to be extremely resistant to coarsening.

Volume fraction untransformed measurements have now been carried out on the specimens of a hypoeutectoid Ti-7%Cr alloy by the point counting technique. As can be seen from the plots in Fig. 7, the percentage of α phase present in these samples at a given temperature approached a constant value which was found to be quite accurately equal to that predicted by application of the Lever Rule to the $\alpha+\beta$ region or its metastable equilibrium extrapolation. The eutectoid isotherm in the Ti-Cr system occurs at 940 K. It is significant that even at lower isothermal reaction temperatures the volume fraction of the α phase approaches a constant value, indicating that the $\alpha+\beta$ microstructure is able to achieve metastable equilibrium (as originally shown by Frost et al (22)). In Fig. 8, the experimentally determined equilibrium (stable and metastable) volume fraction of the α phase at various temperatures is plotted and compared with the values predicted from the phase diagram by application of the Lever Rule. A discontinuity in the experimental data is evident at 893-898°K. Before comparing the experimental data with the calculated curves, we must pause to examine the Ti-Cr phase diagram in more detail.

The β solid solution in titanium alloys is usually associated with a large positive deviation from ideality. This fact has been experimentally verified by direct thermodynamic measurements (23) in Ti-Cr and also by indirect methods in several binary titanium alloy such as Ti-V and Ti-Mo (24-29). One manifestation of the thermodynamic nature of the β phase is the development of a miscibility gap, either stable (as in Ti-Mo (25)) or metastable (in Ti-V, Ti-Nb, Ti-Cr etc.), resulting

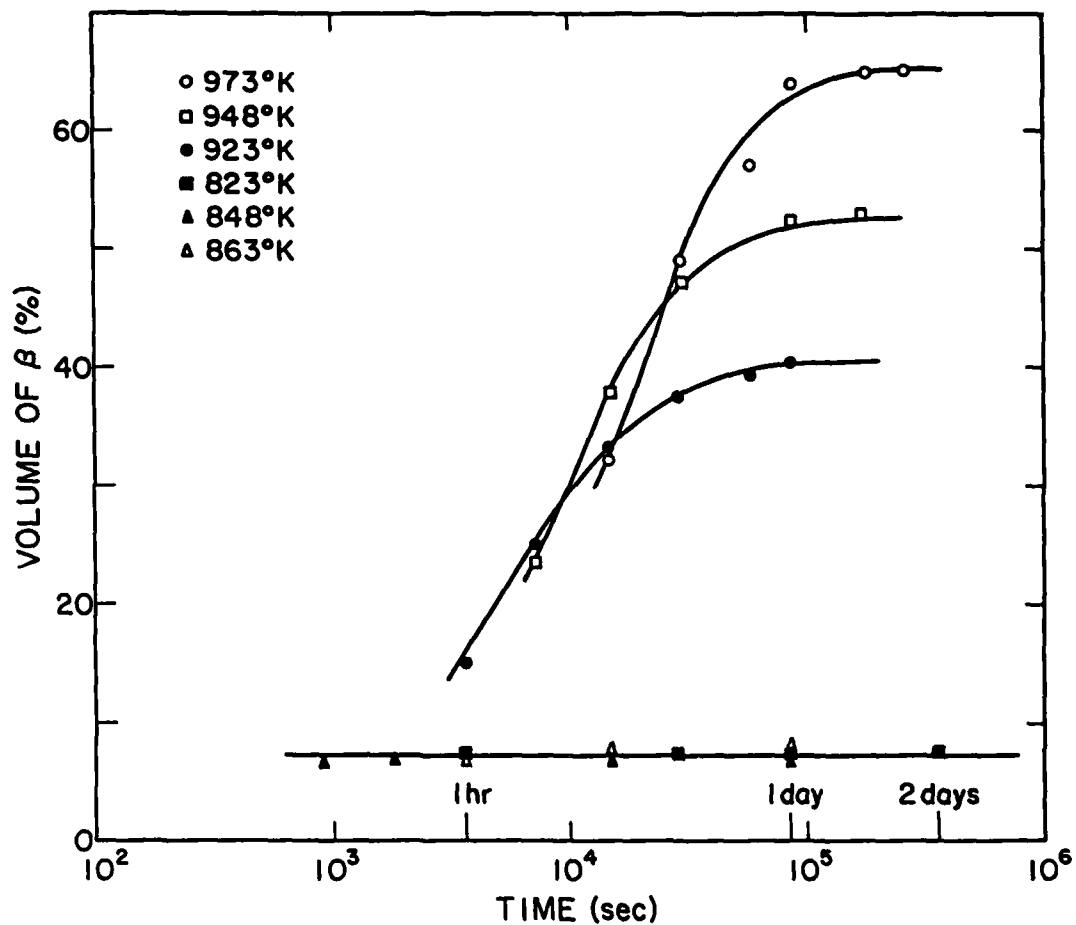


Figure 7: Ti-6.6 at %Cr, β -solutionized and isothermally reacted at indicated temperatures. Plot of volume of β phase untransformed as a function of holding time at the isothermal reaction temperature.

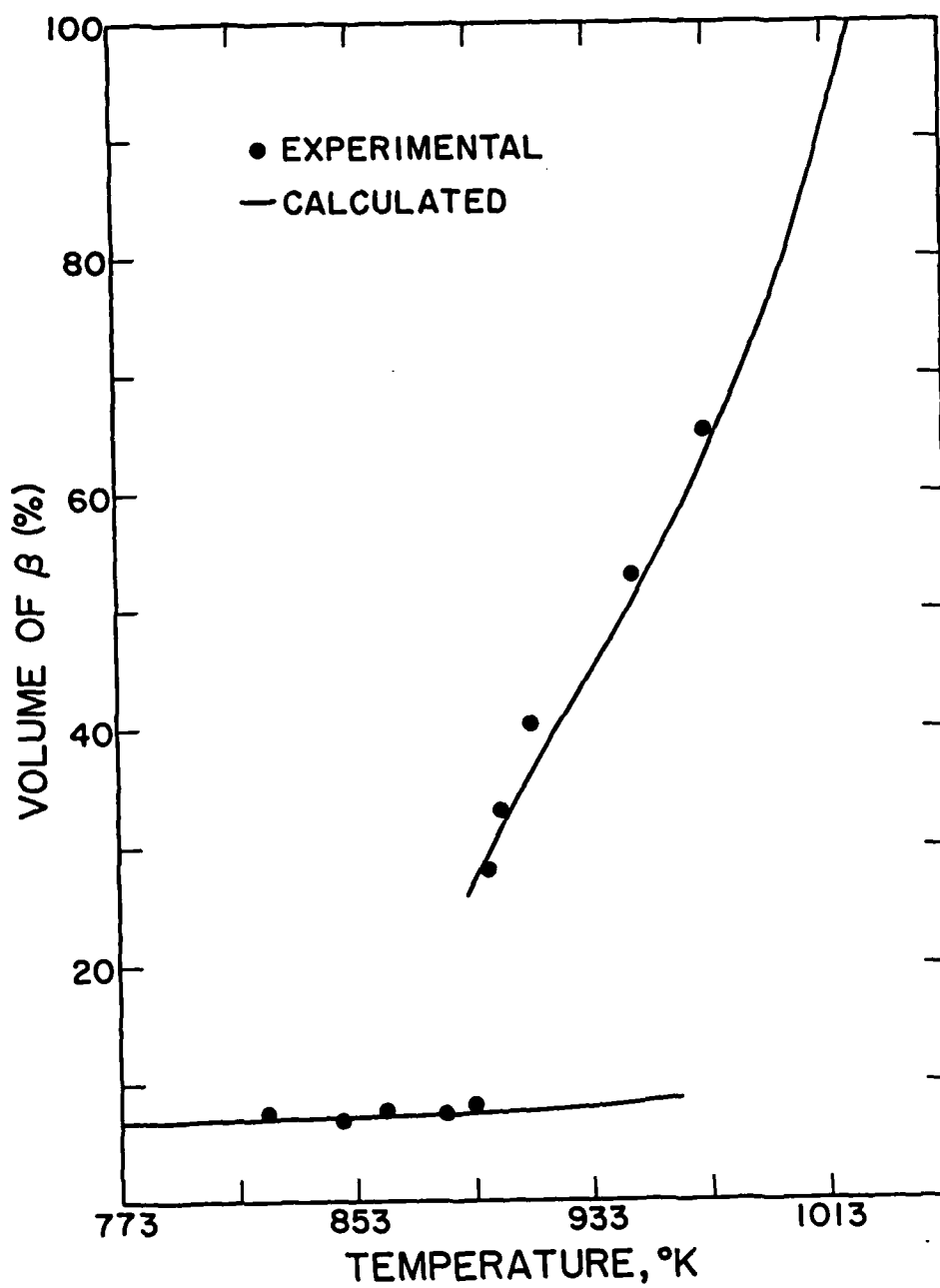


Figure 8:

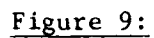
Ti-6.62 at % Cr. Equilibrium or metastable equilibrium volume fraction of β phase as a function of temperature. The continuous line was calculated from the phase diagram by means of the Lever Rule.

in the monotectoid reaction, β (Ti-rich) $\rightarrow \alpha + \beta_2$ (solute-rich). The Ti-Cr system is characterized by the following excess free energy functions (29):

$$G^{\beta \text{ excess}} = x(1-x) [24667 - 6.7 T - 300(1-2x)] \quad [19]$$

$$G^{\alpha \text{ excess}} = x(1-x) [43403] \quad [20]$$

The metastable equilibrium diagram of the Ti-Cr system was calculated and is superimposed on the equilibrium phase diagram in Fig. 9. The metastable monotectoid reaction and the chemical spinodal boundary are also shown and it can be seen that the metastable extensions of the $\beta / (\alpha \beta)$ boundary terminate at the spinodal boundaries. A similar construction has been previously reported by Cahn (30). As pointed out by Menon et al (31), below a certain temperature, a common tangent cannot be constructed between the free energy-composition curves of the α phase and the Ti-rich portion of the β phase and that the spinodal composition delineates the richest composition from which such a common tangent construction can be made. This is easily seen from the G-X diagrams drawn at two different temperatures shown in Fig. 10. In this figure it may be noticed that while two common tangents can be constructed between the G^{α} and the G^{β} curves at 950K, only one such tangent can be drawn at 850K. The effect of the positive excess enthalpy of the β phase in Zr alloys upon the sequence of phase transformations has been examined in detail and experimentally verified (31-35). The present experimental result also appears to be a direct consequence of the thermodynamics of the β phase. The shift from the $\alpha - \beta_1$ equilibrium to the $\alpha - \beta_2$ equilibrium results in an increased driving force for the precipitation reaction, such as could account for the accelerated growth rate of black plates; this shift should also be responsible for the discontinuous and drastic drop in the metastable equilibrium proportion of untransformed shown in Fig. 8. The large change in the lattice parameter of the β phase, from 0.3283 nm at Ti-6.62 at. % Cr to 0.883 nm at Ti-84 at. % or (corresponding to the high-Cr termination point of the metastable monotectoid



Phase Diagram of the Ti-Cr system.

- stable equilibrium phase boundaries
- metastable equilibrium boundaries
- .-. spinodal boundaries
- metastable extension on $\beta | \alpha + \beta$ boundary
- ... metastable $\alpha + \beta$ boundary

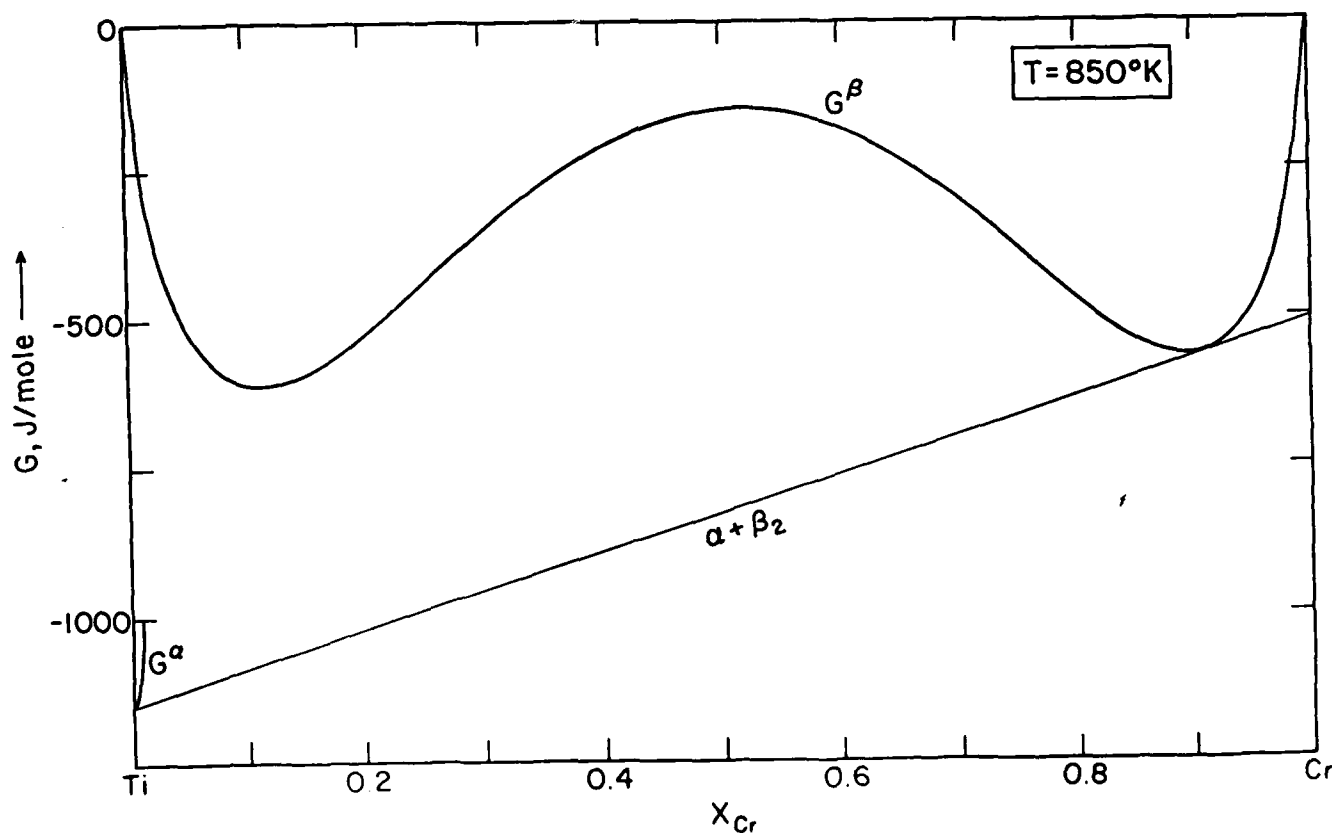
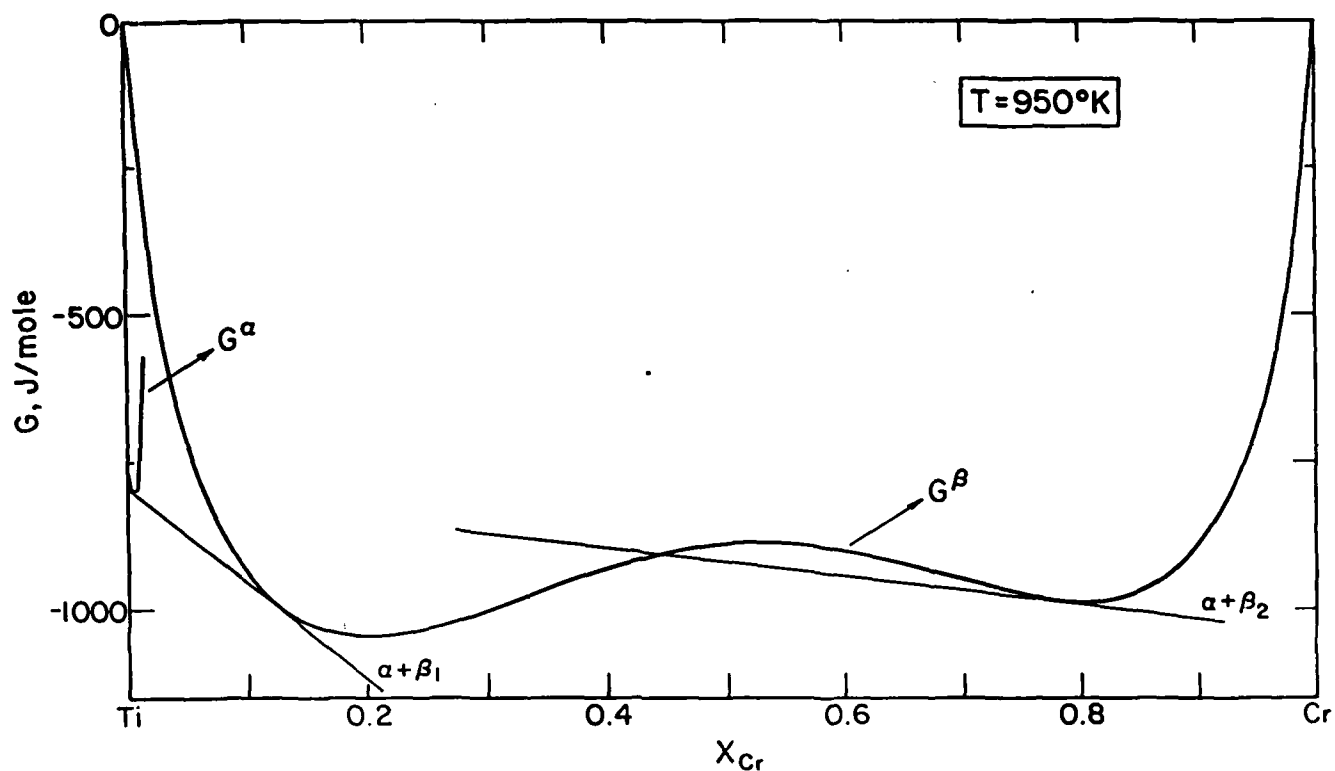


Figure 10: Free energy composition diagrams showing G^α and G^β curves. (a) At 950°K, Common tangents for the α - β_1 stable equilibrium and the α - β_2 unstable equilibrium can be constructed (b) At 850°K only the α - β_2 metastable equilibrium can be obtained.

invariant line), would lead to a large difference in the $\alpha:\beta$ interfacial structure, and hence possibly in morphology as well. We are currently carrying out a detailed structural analysis of the $\alpha:\beta$ interface by means of TEM in order to test this prediction. The interfacial structures of the broad faces of both normal α and black plates are being studied.

The calculations predict the transition from $\alpha-\beta_1$ metastable equilibrium to $\alpha-\beta_2$ metastable equilibrium to occur at 891 K while the experimentally observed transition temperature is about 6 K higher. This rather small difference may be real, and perhaps due to the fact that a higher oxygen content in the alloy studied relative to that on which thermodynamic measurements were made would increase the relative stability of the α phase, resulting in a higher transition temperature. This hypothesis is further strengthened by the observation(36) that the addition of 4% Al (Al is a strong stabilizer) to a Ti-10% Mo alloy raises this transition temperature by about 75°.

On the basis of these considerations, it is concluded that the black plates found in many Ti alloys probably result from the abrupt shift in the metastable equilibrium compositions of the two participating phases, α and β . This derives from the thermodynamic nature of the β solid solution.

E. Influence of Beta Grain Size upon Proeutectoid Alpha Morphology

This investigation will become the Ph.D. thesis research of Miss Amber Dalley. Her tuition and stipend are being funded by the CMU Department of Metallurgical Engineering and Materials Science; her consumable supplies are furnished by the present grant.

Investigations by Dr. F.H. Froes and co-workers (37) at Wright-Patterson Air Force Base have shown that replacing the Widmanstätten morphologies of proeutectoid alpha with grain boundary allotrimorphs significantly improves fatigue properties.

This replacement was accomplished through the development of very small beta grain sizes as a result of the presence of finely distributed porosity and/or inorganic particles remaining from the alloy manufacturing process. This effect, though still not formally recognized in the titanium alloy literature, has been known for more than a century in connection with the proeutectoid ferrite reaction in steel. However, the detailed growth mechanism through which this is achieved, though discussed theoretically in some detail (38), has not been properly investigated experimentally because of destruction of the austenite matrix in steel by the martensite transformation during quenching to room temperature. Hence the changes in the interphase boundary structure, particularly with respect to growth ledges, which are expected to attend reductions in matrix grain size, cannot be studied. In this investigation, we propose to transfer the steel problem to the proeutectoid alpha reaction in Ti-X alloys (probably emphasizing the Ti-Cr system), taking advantage of the convenient retainability of the beta matrix to make the requisite high-resolution TEM studies of interphase boundary structure as a function of β grain size. Miss Dalley's study will thus make full use of Mr. Menon's investigation of proeutectoid alpha:beta boundary structure in coarse-grained Ti-Cr alloys, and build further upon it. Emphasis will also be placed on gathering quantitative data on the influence of beta grain size upon the W_s (Widmanstätten-start) temperature as a function of alloy composition. This latter set of results should be of considerable practical interest to the titanium alloy development programs in Dr. Froes' group.

This study will be conducted in collaboration with Dr. F.H. Froes. During the P.I.'s first visit to Dr. Froes' group he was delighted to learn that rapid quenching techniques, e.g., melt spinning, can yield beta grain sizes as small as 100 nm. Dr. Froes indicated that these grain sizes are relatively stable, though manipulable, since the beta grains extend entirely through the thickness dimensions of the foils in which they are formed and hence their boundaries tend to be anchored at the foil

surfaces. We have accordingly requested that Dr. Froes' operation supply a quantity of Ti-7% Cr rapidly quenched microcrystalline foil upon which Miss Dalley can begin her investigation. In the meantime, she is taking the coursework and accomplishing the literature reading needed to provide a sound basis for her research. She has also learned the heat treatment techniques used in our group for titanium-base alloys and has begun to acquire proficiency in transmission electron microscopy. This technique, supplemented by optical microscopy, will be the principal experimental tool used during her thesis research.

III. The Bainite Reaction

This program is the Ph.D. thesis research of Mr. Hwack Joo Lee.

A. Surface Relief Effects

Three definitions of bainite are currently in use, each referring to a different set of phase transformations phenomena (1). In this program, the "generalized microstructural" definition of bainite (1,6) is being employed: bainite is the product of a non-lamellar, non-cooperative (2) mode of eutectoid decomposition. Hence precipitation of intermetallic compound as well as of alpha is important. However, the most widely accepted definition of bainite at the present time is the "surface relief" definition. Stating this in modernized fashion, bainite consists of precipitate plates which grow by shear at rates paced by diffusion; slow growth rates indicate the participation of diffusion in the transformation process, whereas an invariant plane strain surface relief effect "proves" that shear also plays a significant role. The particular facet of the arguments surrounding this definition with which this portion of our program deals is that of the morphology of the surface relief effect. As Wayman (39) has pointed out, one of the requirements which a product phase crystal must fulfill exactly if it is to be eligible for classification as the product of a martensitic transformation is that the relief effect which it

produces when formed at a free surface be of the invariant plane strain type. Indeed, product phase plates which are indisputably formed by a martensitic or shear mechanism do produce just this effect. However, a considerable variety of effects in addition to the invariant plane strain (IPS) morphology have been found to accompany formation of slowly growing precipitate plates (39, 40-42). Advocates of a shear mechanism for the formation of such plates have utilized a variety of explanations in an attempt to rationalize non-IPS effects within the framework of a shear mode of transformation. The simplest and one of the most common non-IPS relief effects is tent-shaped. The simplest shear-oriented explanation for this relief is that it consists of two plates formed back to back (39,43). For the particular case of proeutectoid ferrite plates in steel, this explanation has been refuted by optical microscopy and thermionic electron emission microscopy observations (2) and by the Kossel micro-diffraction technique(44). Recently, however, TEM evidence has been introduced for the back-to-back plates explanation (45). This finding is likely due to incompetent heat treatment of an Fe-C alloy, such that second plates were able to nucleate sympathetically in the back-to-back configuration at those formed initially as a consequence of insufficiently rapid quenching from the transformation temperature to room temperature (46). However, transformations in interstitial alloys do not always provide the most decisive models for testing shear mechanisms because the possibility is said to exist that the substitutional atoms can undergo a lattice transformation by shear while the interstitials can be partitioned diffusively between the product and matrix phase without markedly affecting the mechanics of shear (47). Accordingly, we have undertaken to repeat the surface relief and TEM experiments on a Ti-7.15% Cr alloy in order to take advantage of the substitutional character of both parent and product phases during the formation of proeutectoid alpha plates.

Specimens with a prepolished surface which had then been carefully cleaned were wrapped in a Ta foil and then Vycor encapsulated in vacuo. Following a solution annealing treatment of 20 min. at 1000 C, they were isothermally reacted at 687 C, a temperature not far above that of the eutectoid; quenching was performed by immersing the capsules, unbroken, in iced brine.

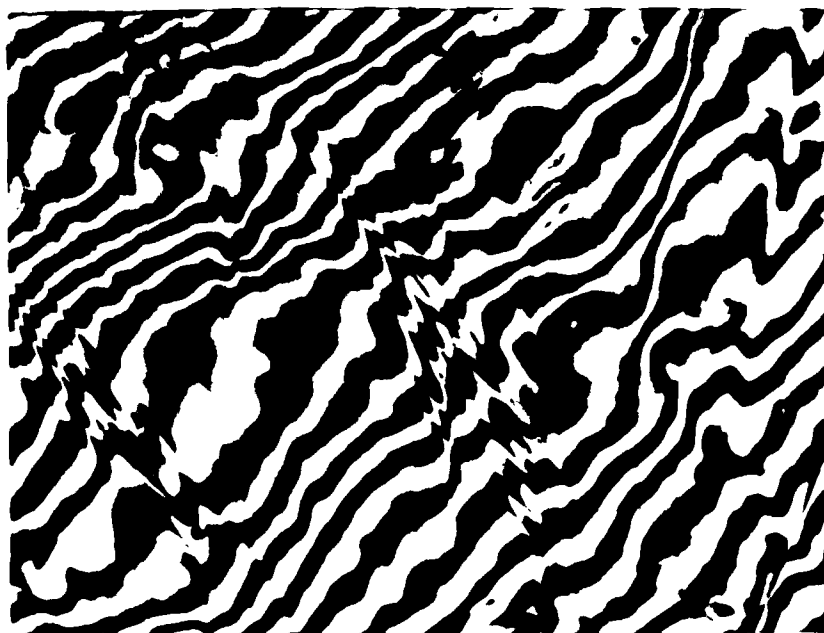
Fig. 11a shows proeutectoid alpha sideplates with bright field illumination in a specimen reacted 70 min. at 687 C; the same area is shown in Fig. 11b photographed with the Nomarski differential interference technique under xenon illumination. Close inspection of Fig. 11b indicates that all alpha plates exhibit a tent-shaped relief effect. In Fig. 12 the same specimen is imaged in TEM after thin foil preparation; Fig. 12b shows in dark field the same area as is displayed in bright field in Fig. 12a. The selected area diffraction pattern of Fig. 13 confirms that the product phase is alpha and that it exhibits the usual Burgers orientation relationship with respect to beta. (Extra spots in this diffraction pattern are due to the omega phase (48).) Figs. 12 and 13 make clear that each alpha plate is a single crystal. There is no evidence of back-to-back formation of alpha plates. Despite the relatively slow cooling rates permitted within an evacuated Vycor capsule, the transformation kinetics were slow enough to permit avoidance of the sympathetic nucleation of additional plates during quenching to room temperature.

Hence clear-cut evidence is presented that tent-shaped surface relief effects are produced by single, slowly growing (49) precipitate plates formed in a substitutional solid solution. On the phenomenological theory of martensite (39), these plates cannot have formed by shear. The implications of this quite definite result with respect to the transformation mechanism of ferrite and bainite plates in steel which also yield a tent-shaped surface relief effect is obvious.



a

25um



b

Figure 11



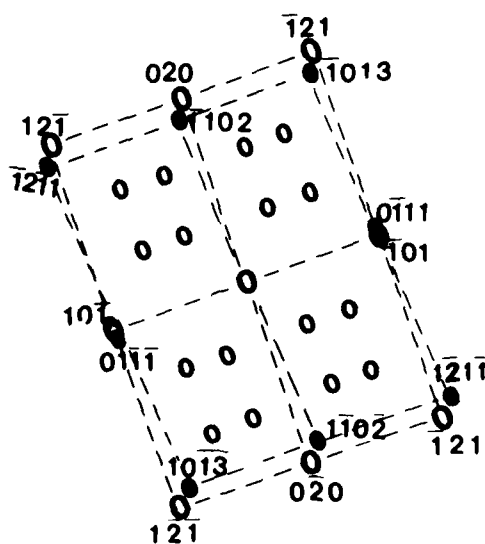
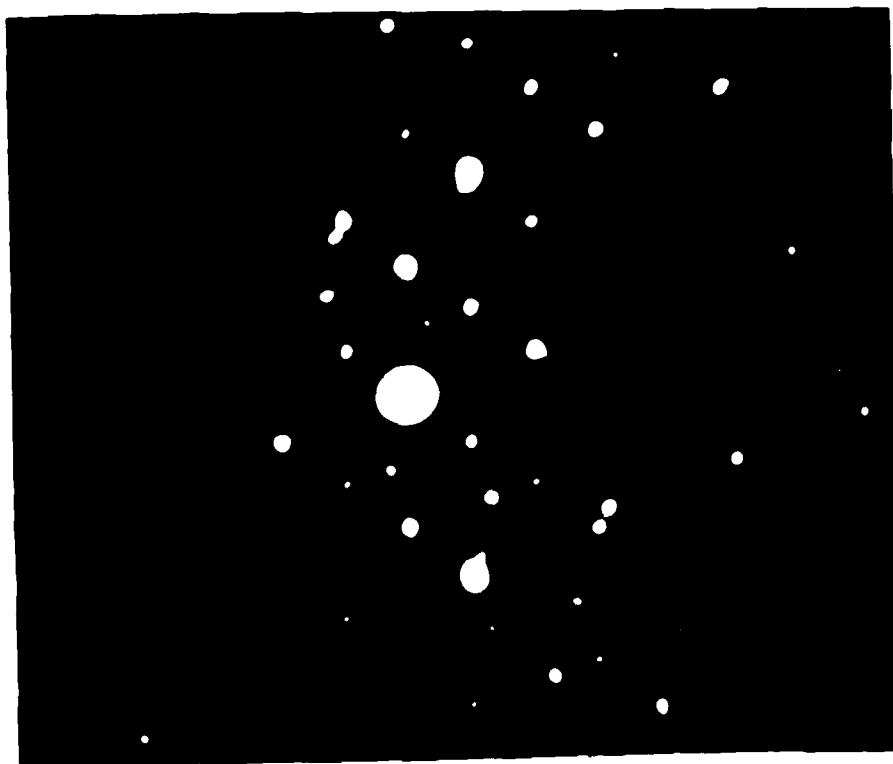
a

.5um



b

Figure 12



Z.A.
 $\circ \beta [101]$
 $\bullet \alpha [5143]$
 $\circ \omega$

Figure 13

B. Morphology, Crystallography, Growth Kinetics and Mechanism of Bainite Nodule Formation in a Hypereutectoid Ti-Cr Alloy

1. Introduction

One of the original objectives of this program was to conduct a detailed investigation of bainite nodule formation. Such nodules were reported in 1957 in a high-oxygen Ti-10.64% Cr alloy (5). During the recent investigation of Franti et al (6), however, it was noted that: (a) bainite nodules do not form to a significant extent in hypoeutectoid alloys in any of the other nine Ti-X systems in which the proeutectoid alpha and then the bainite reaction occur instead of the massive alpha transformation, and (b) even in the lower oxygen Ti-Cr alloys now available nodule formation is not pronounced. Evidently coarsening of the Widmanstätten alpha structure occurs more rapidly in the presence of higher oxygen concentrations. Coarsening makes available sufficiently large contiguous volumes of beta which are free of alpha plates in the vicinity of the beta grain boundaries so that bainite nodules nucleating at grain boundary alpha allotriomorphs are able to develop in readily recognizable form. When bainite formation begins before this much coarsening has occurred, the nodules simply fill in the plate-like volumes of beta which remain between closely spaced proeutectoid alpha plates. Presumably the mechanism of the transformation is the same but the morphology of the nodules thus formed does not lend itself well to either measurement or analysis.

Recalling another early Air Force-sponsored investigation of transformations in Ti-Cr alloys, this time in a hypereutectoid alloy (50), it was noted that bainite nodules in this composition range develop much more readily because proeutectoid TiCr_2 plates form far less voluminously and much more slowly than proeutectoid alpha plates do in hypoeutectoid alloys. Two hypereutectoid Ti-Cr alloys were accordingly purchased from Timet, Henderson, NV., through the courtesy of Dr. J.A. Hall,

and did indeed prove satisfactory for an investigation of bainite nodule formation.

All of the studies reported here were conducted on a Ti-25% Cr alloy reacted at 665 C. Extension of these studies to other reaction temperatures is presently in progress.

2. Bainite Nodule Morphology

a. Optical Microscopy Studies

Fig. 14a shows a variety of bainite nodule shapes along a beta grain boundary at which precipitation began by formation of proeutectoid TiCr_2 sideplates. Others evolved in approximately hemispherical fashion. In Fig. 14c, impingement is seen to have converted the bainite structure into an optically almost unresolvable "sheet", thickening about uniformly normal to the grain boundary. Fig. 15 indicates that the details of bainite nodule morphology vary, as expected, from one grain boundary to the next; however, these variations are not very large, and likely reflect primarily variations in proeutectoid TiCr_2 morphology. Fig. 16 shows intragranular TiCr_2 plates gradually being engulfed by bainite nodules.

b. SEM and TEM Studies

Fig. 17 is an SEM micrograph of bainite nodules developed at a beta grain boundary in the Ti-25% Cr alloy reacted for 1 hr. at 665 C. The TiCr_2 crystals are seen to be largely non-lamellar and quite irregular in shape. Sideplate nodules have developed into the "upper" beta grain and spherical nodules into the "lower" one, indicating that crystallography probably determines the type of nodule developed. Note that TiCr_2 does not occupy completely the beta grain boundary. Eutectoid alpha is in contact with some areas of this boundary. Fig. 18 illustrates intragranular bainite nodules in the same specimen. Both sideplate and spherical nodules are present, with the overall morphologies being reminiscent of "inverse bainite" in hypereutectoid steels (2).

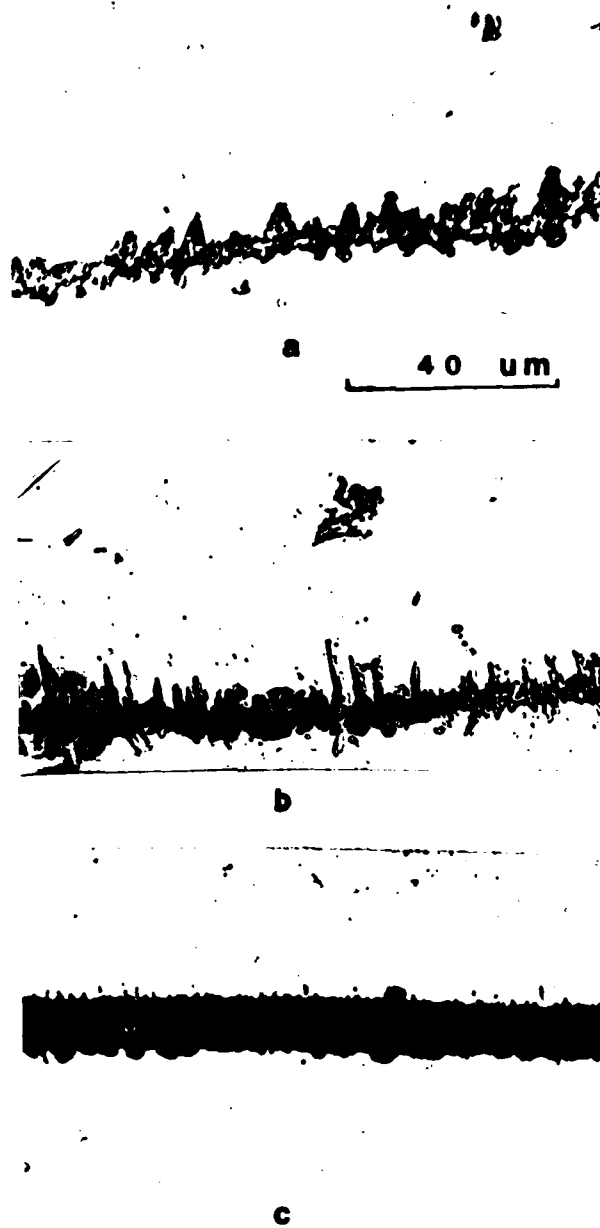


Figure 14

40 μm



Figure 15

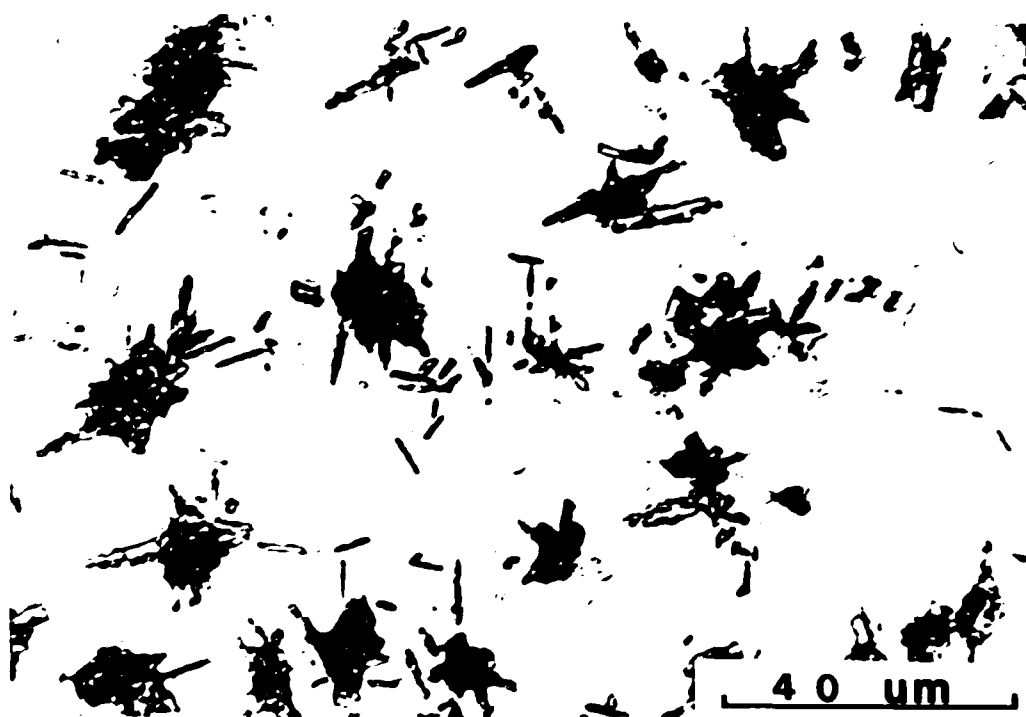


Figure 16

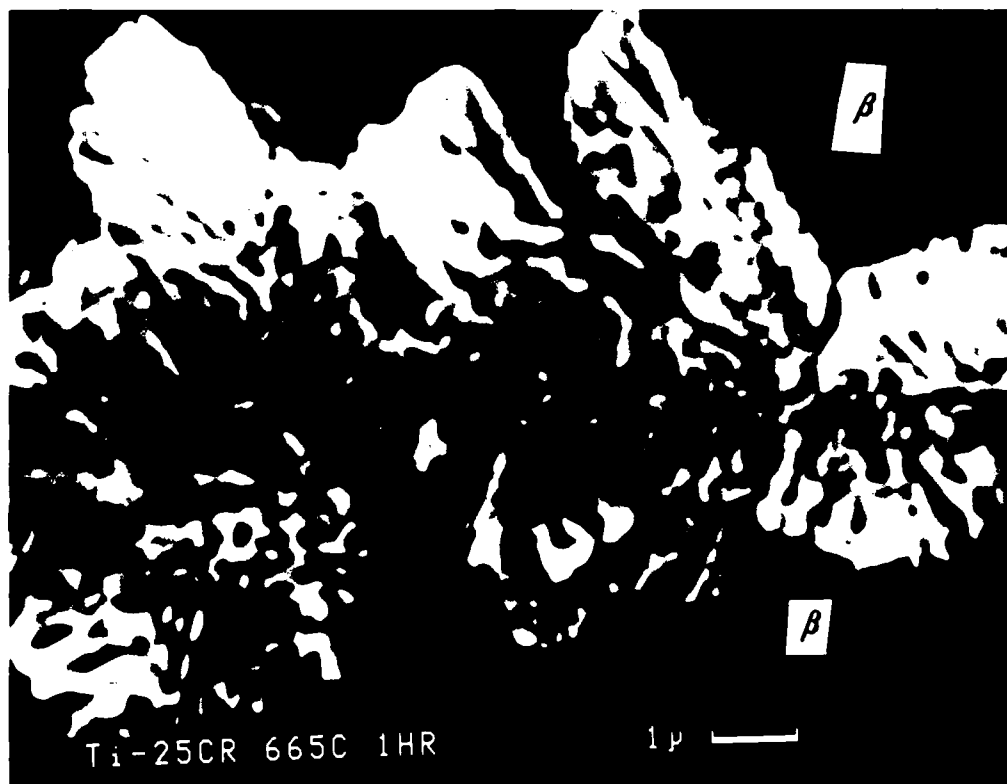


Figure 17

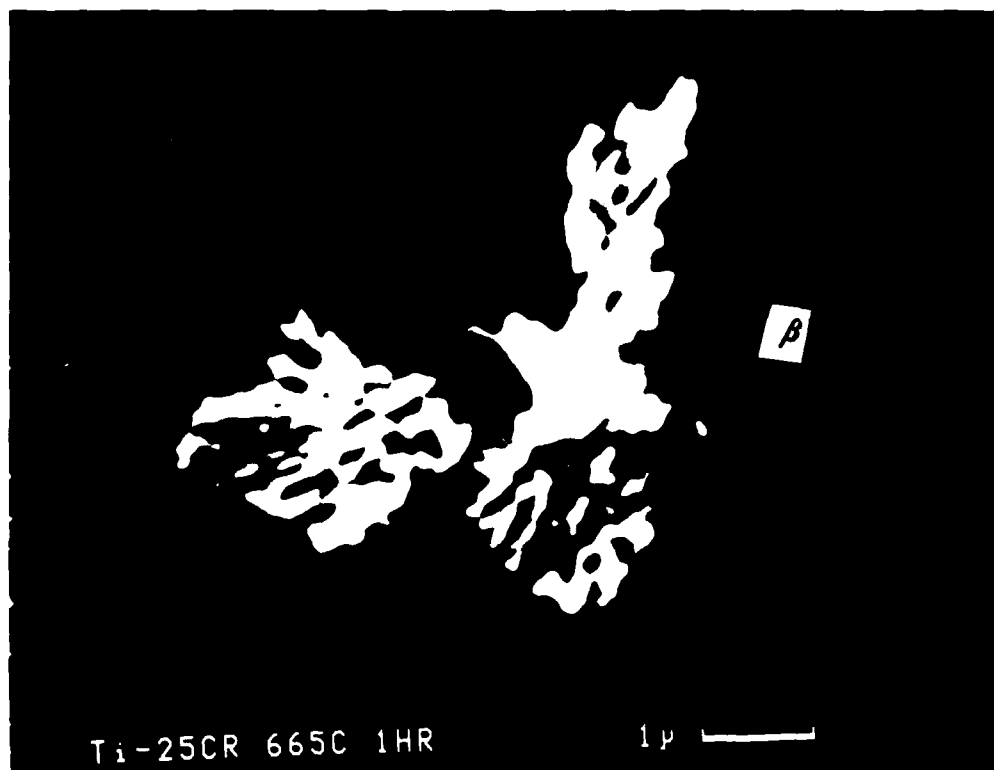


Figure 18

Figs. 19 and 20 are bright-and-dark field micrographs, respectively, of the same area, a portion of a bainite nodule. Misfit dislocations are observed at both α : β and TiCr_2 : β interfaces; they are spaced ca. 15 nm. apart at the former boundaries and somewhat more widely and irregularly at the latter. Fig. 21 is a magnified view of a portion of Fig. 20 (dark field), illustrating more clearly facets on TiCr_2 : β interfaces. This set of micrographs thus shows that, in accord with expectation from nucleation theory (51) but not with recent (unsubstantiated) views of equivalent microstructures in alloy steels (52), that the irregularly shaped bainite nodules are composed of α and TiCr_2 crystals which are apparently largely if not entirely enclosed by partially coherent interphase boundaries. Quantitative characterization of these structures is now being attempted.

Fig. 22 is a bright field TEM micrograph of a sideplate-type bainite nodule. Note that interphase boundaries are again partially coherent; the features which are ledges remain to be distinguished from those which are misfit dislocations (and possibly Moire fringes). Note that "cooperation" between growth of α and TiCr_2 is distinctly poorer than in the case of pearlite. Unlike bainite in hypoeutectoid steels, the intermetallic compound and α phases are present in similar proportions. Different from both ferrous bainite and pearlite are also the observations that TiCr_2 is in contact with the (β) matrix on one side of the nodule and α is so positioned on the other. Hence the combined nucleation and growth rates of the two phases are presumably roughly comparable rather than widely disparate as in steel.

3. Bainite Nodule Crystallography

TEM was used to evaluate the crystallography of the bainite nodules.

As in our previous reports,

$$(0001)_{\alpha} // (110)_{\beta} // (111)_{\text{TiCr}_2}$$



Figure 19

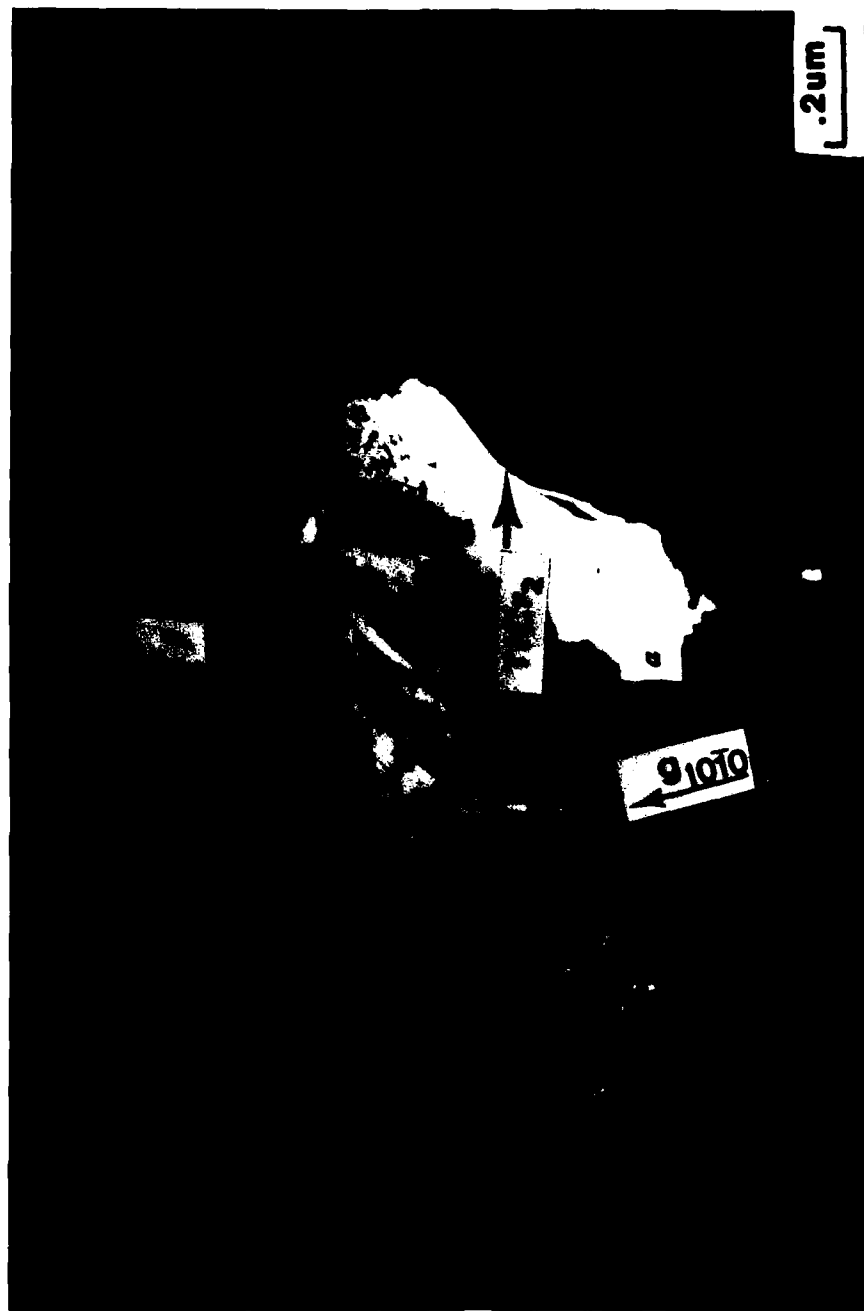


Figure 20

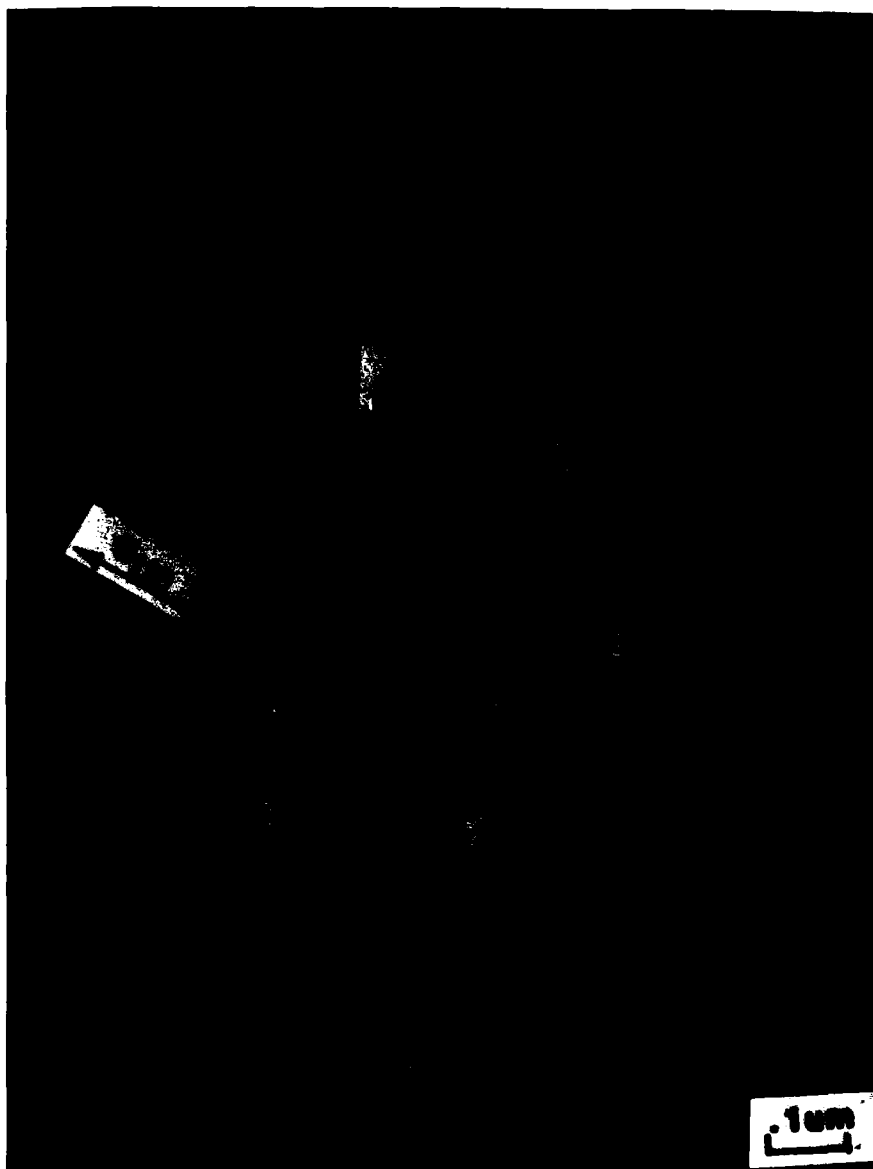


Figure 21



Figure 22

$$[\bar{2}110]_{\alpha} // [11\bar{1}]_{\beta} // [\bar{1}\bar{1}2]_{\text{TiCr}_2}$$

However, at a given grain boundary, a Burgers relationship between α and β normally could and did appear with respect to only one of the two beta grains forming the boundary. In Fig. 23 a Burgers relationship was found between α_1 and β_2 , but not between α_1 and β_1 . Note that α_1 grew preferentially into β_1 --an often reported type of result in other transformations (53-55). Fig. 24 shows heavily faceted bainitic alpha, with irregular TiCr_2 crystals "randomly" dispersed within it. Note that the large TiCr_2 crystal in the upper left hand portion of this Figure has just been surrounded by bainitic alpha. In Fig. 25a the beta:bainitic alpha interface exhibits two arrays of orthogonal linear defects, at least one of which is probably misfit dislocations. This boundary also appears to include rather high ledges. Dark-field illumination (Fig. 25b) indicates that the alpha:alpha boundary in this nodule is of the small-angle type. Note also the heavily faceted TiCr_2 crystal just below the center of Fig. 25a. The twins in this crystal were probably formed during ion milling; other damage due to this process (which must be used in order to avoid introduction of the hydrogen-induced interface phase during electrothinning) is evident in Fig. 25b. Fig. 26 displays a small TiCr_2 crystal recently nucleated at a beta:bainitic alpha boundary which subsequently became planar. Close inspection of the TiCr_2 crystal and of the beta:bainitic alpha boundary to the "right" of this crystal suggests again the presence of misfit dislocations. Fig. 27 includes two dark-field micrographs taken of the area shown in Fig. 25. Comparison with Fig. 25 indicates that the various TiCr_2 crystals present have different orientations (though presumably from a common set of orientation relationships). This is a situation different from that of pearlite (56), emphasizing another aspect of the distinctions between lamellar and non-lamellar eutectoid structures. The demonstration in Fig. 28 that a TiCr_2 crystal can protrude far ahead of the beta:bainitic alpha

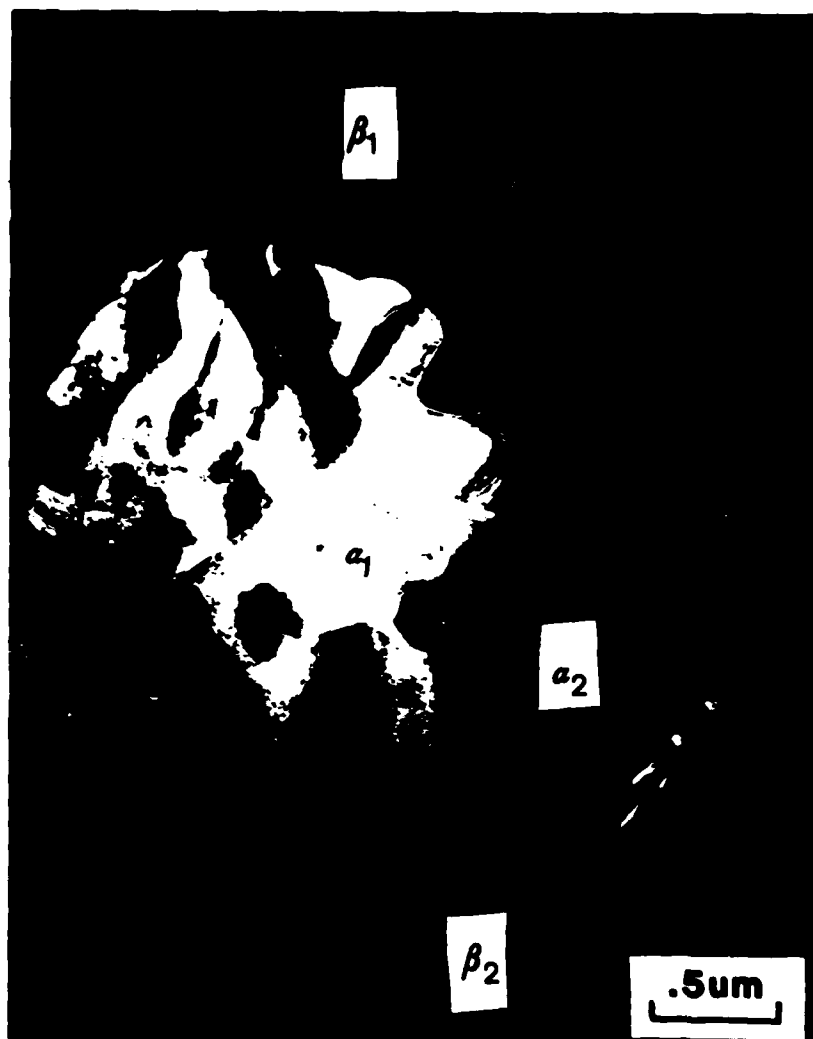


Figure 23

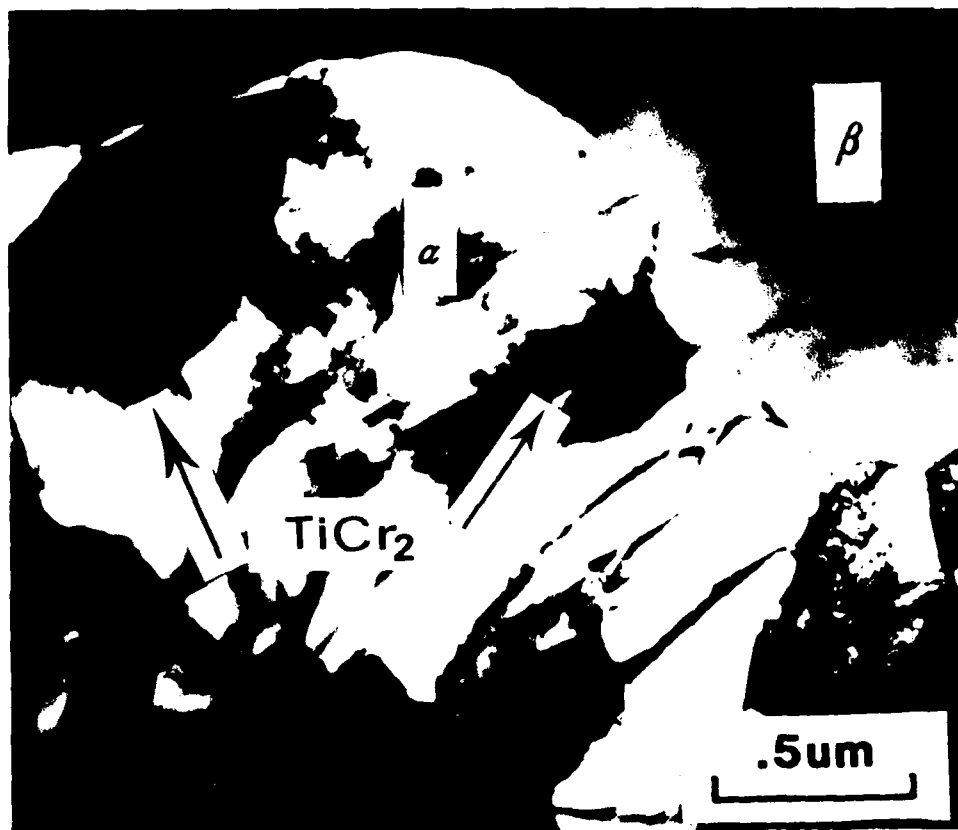


Figure 24

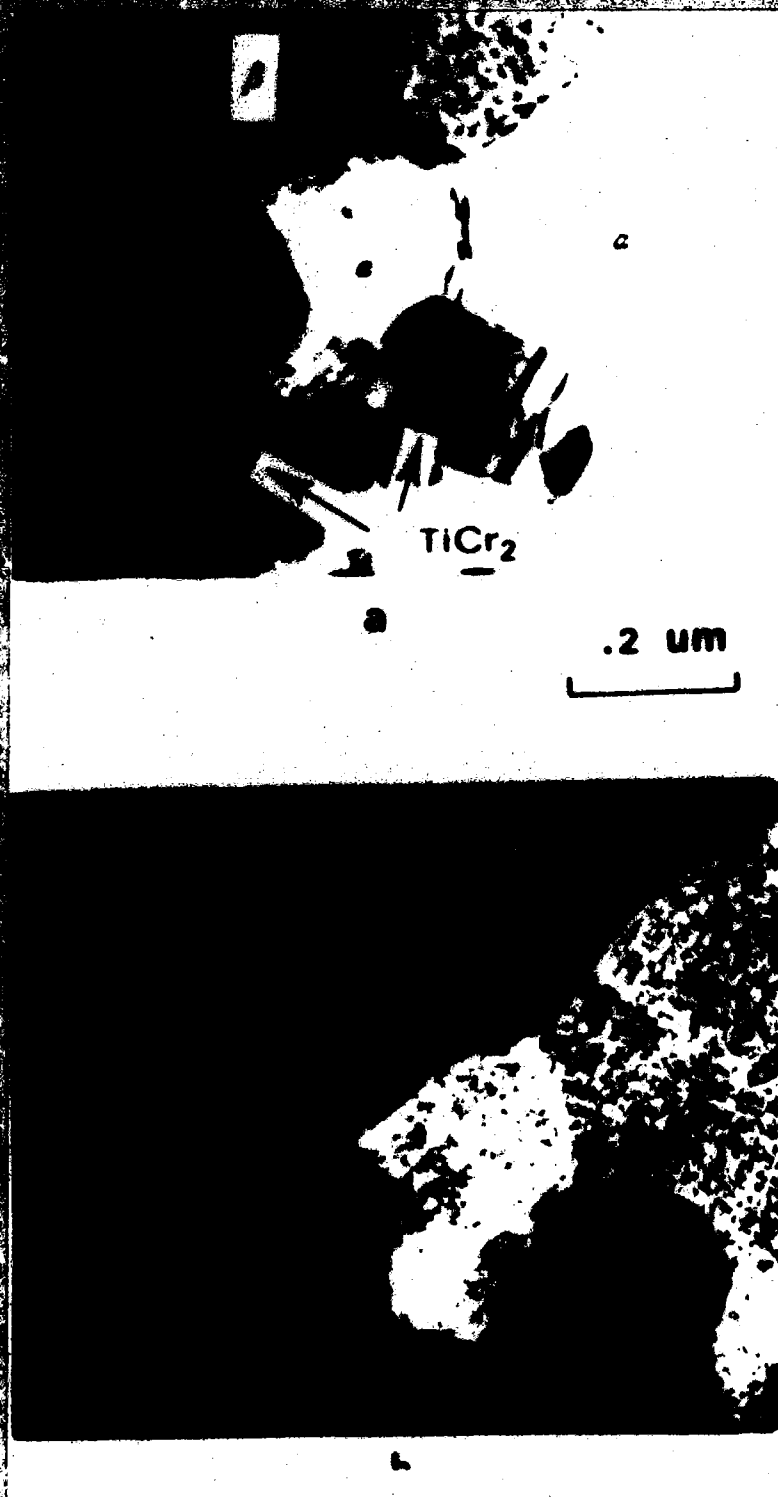


Figure 20



Figure 26



a

2 μ m



b

Figure 27



Figure 28

interface emphasizes another aspect of the non-cooperative nature of the microstructural bainite reaction.

4. Bainite Nodule Growth Kinetics

Fig. 29 shows maximum bainite nodule radius as a function of isothermal reaction time. The slope of this plot is initially constant, diminishing later as a consequence of supersaturation in the remaining beta matrix. This slope corresponds to a growth rate of ca. 0.7×10^{-7} cm./sec. Using a pearlite-like model for the growth rate yields a value of ca. 1.3×10^{-7} cm./sec. Further refinement of the calculation is in progress; at this point in the research, however, it seems safe to conclude that growth of the bainite nodules is controlled by volume diffusion through the matrix phase. This result is consistent with the indications we have reported that the beta:bainitic alpha boundaries are usually partially coherent. Such boundaries are unlikely to provide good paths for "short circuit" diffusion. Extension of these measurements to lower temperatures will be emphasized, however, in order to provide boundary diffusion with better opportunities to become the dominant mechanism.

C. The Proeutectoid Alpha and the Bainite Reactions in Ti-3.9% Co

In this and succeeding subsections, numerous transmission electron micrographs will be presented in which misfit dislocations and growth ledges are displayed. Quantitative characterization of these vital features of interphase boundary structure is just now beginning in both this (the bainite) and in the previous (proeutectoid alpha) sections, and should be a central feature of next year's Annual Report.

The eutectoid temperature and composition in Ti-rich Ti-Co alloys are 685 C and 9.5 W/O Co, respectively. The intermetallic compound in equilibrium with alpha at and below the eutectoid temperature is Ti_2Co , an ordered fcc structure with 96 atoms per unit cell and $a_0 = 1.1306$ nm.

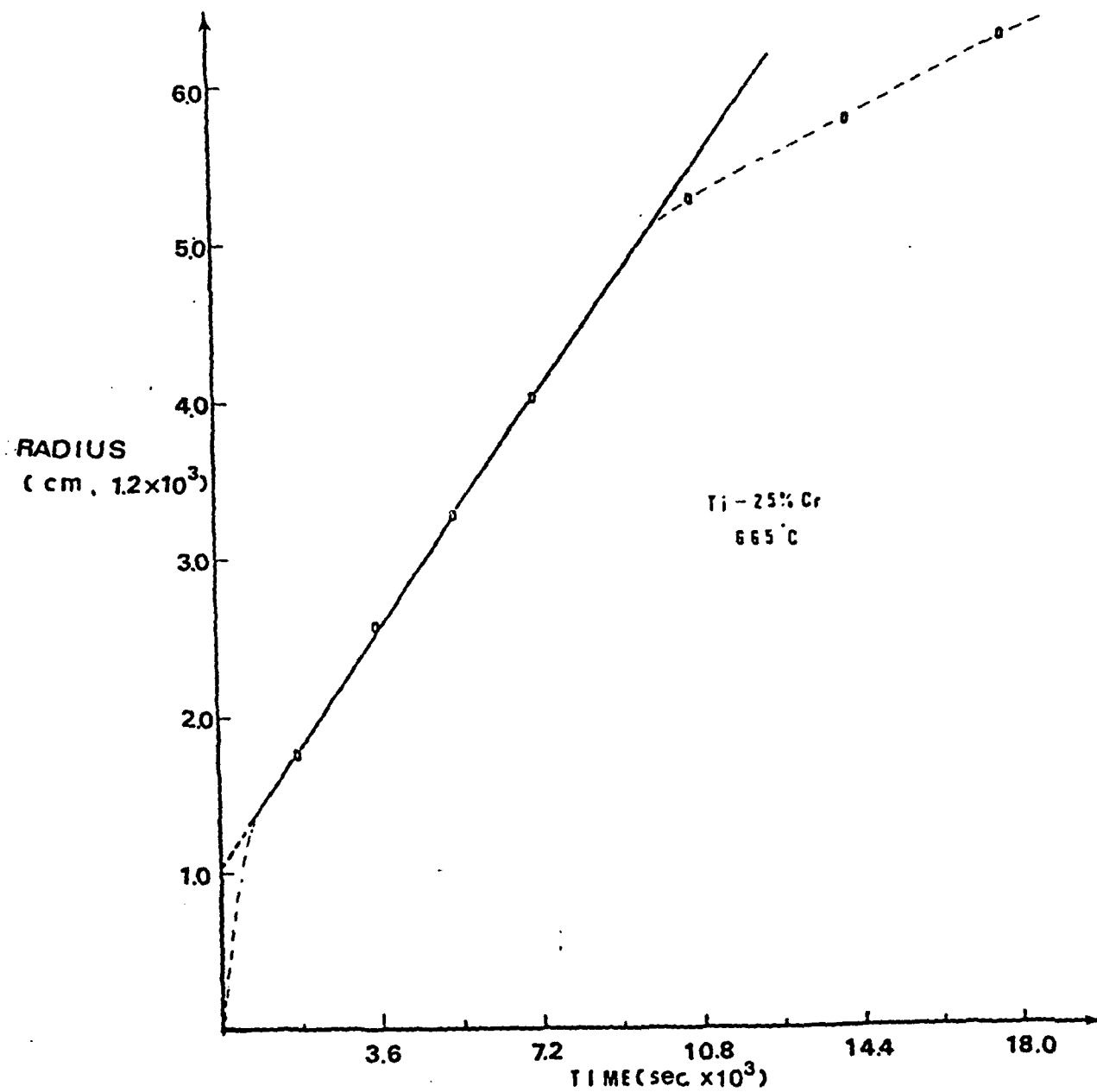


Figure 29

1. The Proeutectoid Alpha Reaction Below the Eutectoid Temperature

We take the bainite reaction in Ti-X alloys to consist of intermetallic compound (or other "second phase") precipitation, initiated at proeutectoid alpha:beta interfaces, followed by further growth, and/or nucleation of additional alpha about the compound crystals thus formed. Hence it is important to examine first the structure of proeutectoid alpha:beta interfaces at which compound nucleation occurs. Much of this work is being undertaken in general fashion as part of Mr. Menon's thesis research, described in Section II. These studies are being supplemented by Mr. Lee in order to assure still closer coupling between them and his concern with formation mechanism of bainitic intermetallic compound crystals.

Fig. 30 and 31 are dark-field images of retained beta, photographed with a $(110)_{\beta}$ reflection (the black background in both micrographs is alpha), in which both misfit dislocations (thin, parallel lines, spaced ca. 10 nm. apart) and growth ledges, thicker black lines, more irregularly spaced, about 40 nm. apart, are clearly revealed. Fig. 31 suggests that more than one array of misfit dislocations is likely to be present. Superledges, each composed of multiple smaller ledges very closely spaced, are also clearly visible and indicated by arrowheads. Fig. 32 is an equivalent dark-field-of- $(110)_{\beta}$ micrograph dramatically displaying the misfit dislocation and ledge structures of the edges of alpha plates (center of the micrograph). In each of a number of areas in this micrograph, the ledges are seen to be producing growth in a quite specific direction. Arrowheads indicate locations where misfit dislocations are most clearly visible, again spaced ca. 10 nm. apart.

2. The Bainite Reaction in Ti-3.9%Co

Figs. 33-35 were taken of the same area, in bright field (Fig.33), and in dark field with an $(020)_{\text{Ti}_2\text{Co}}$ reflection (Fig.34) and with a $(200)_{\beta}$ reflection (Fig. 35), respectively, at a specimen reacted for 40 min. at 625 C. Fig. 36 is a



Figure 30

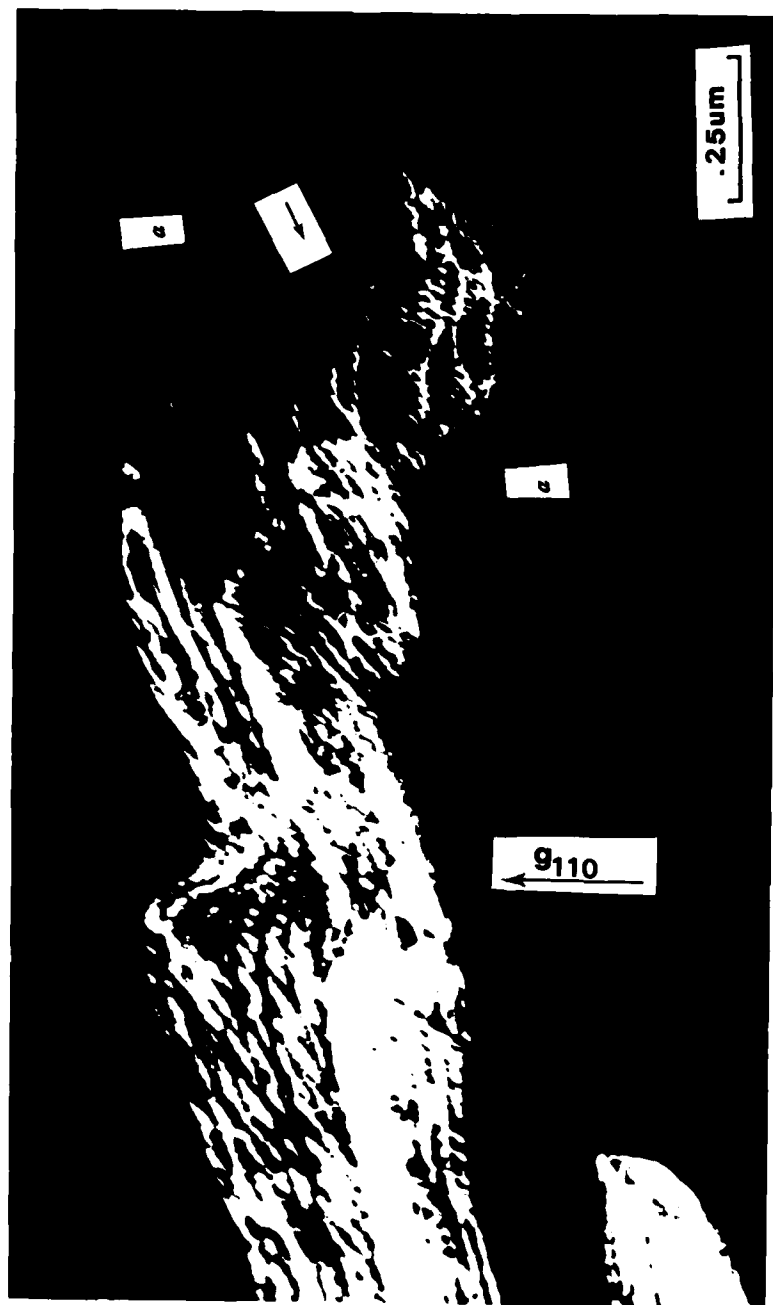


Figure 31

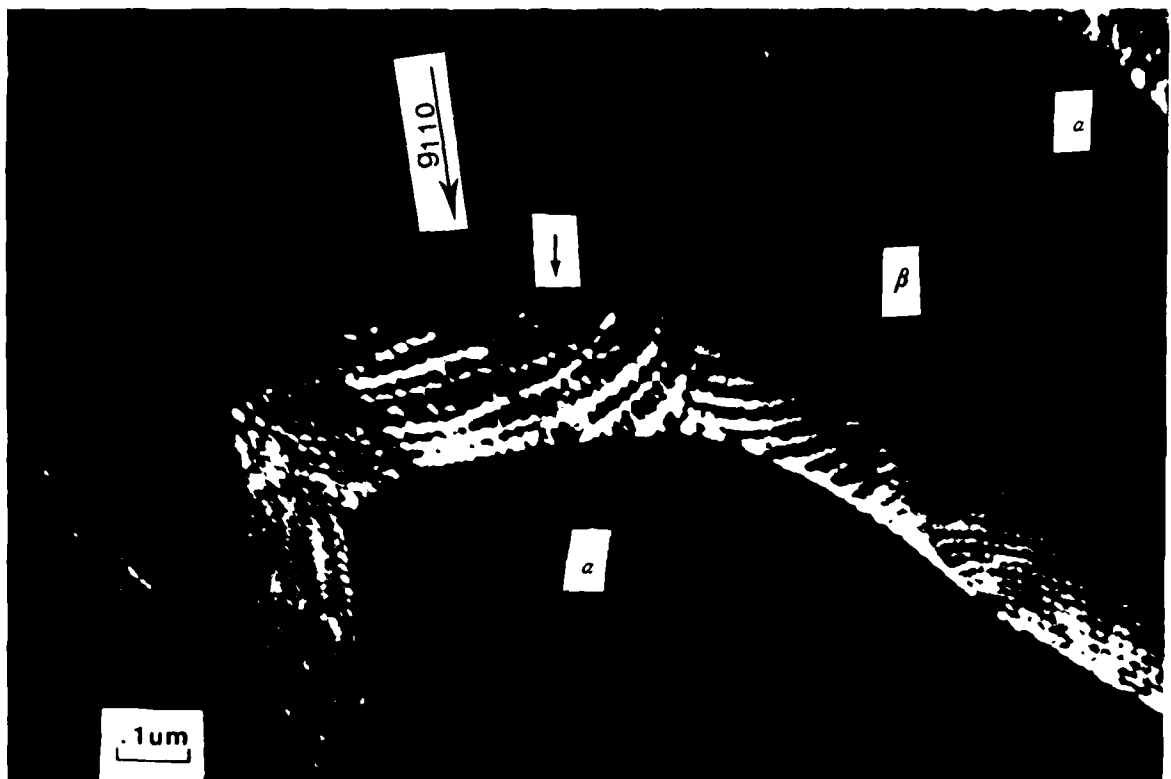


Figure 32



Figure 33

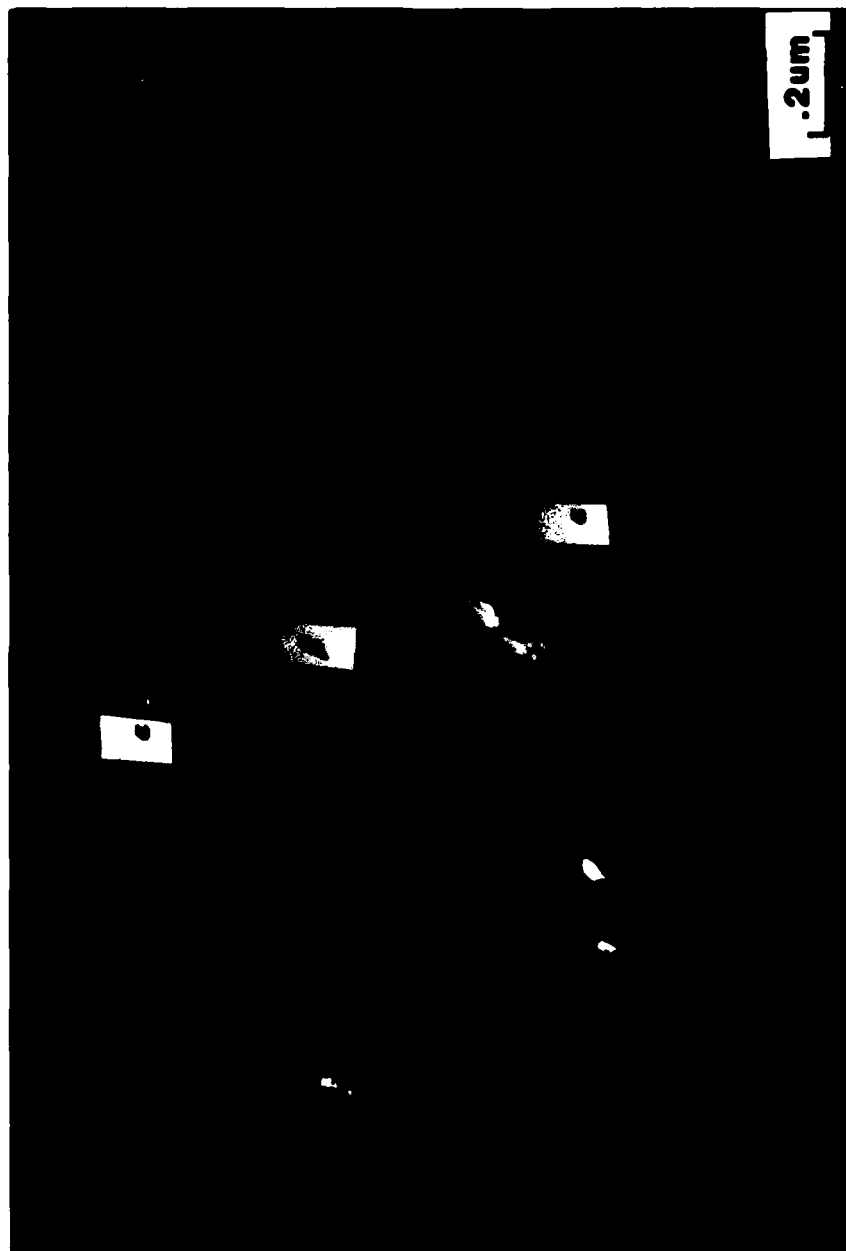
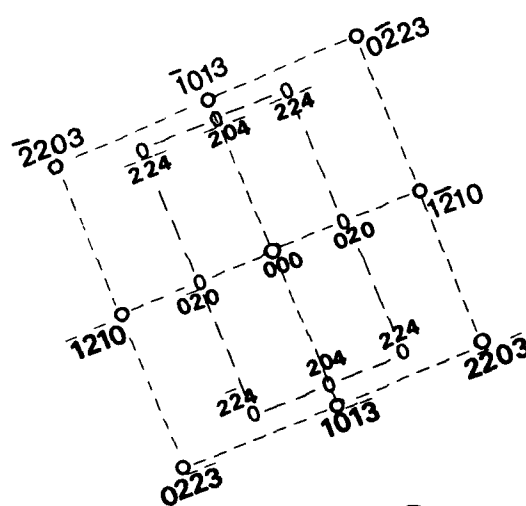
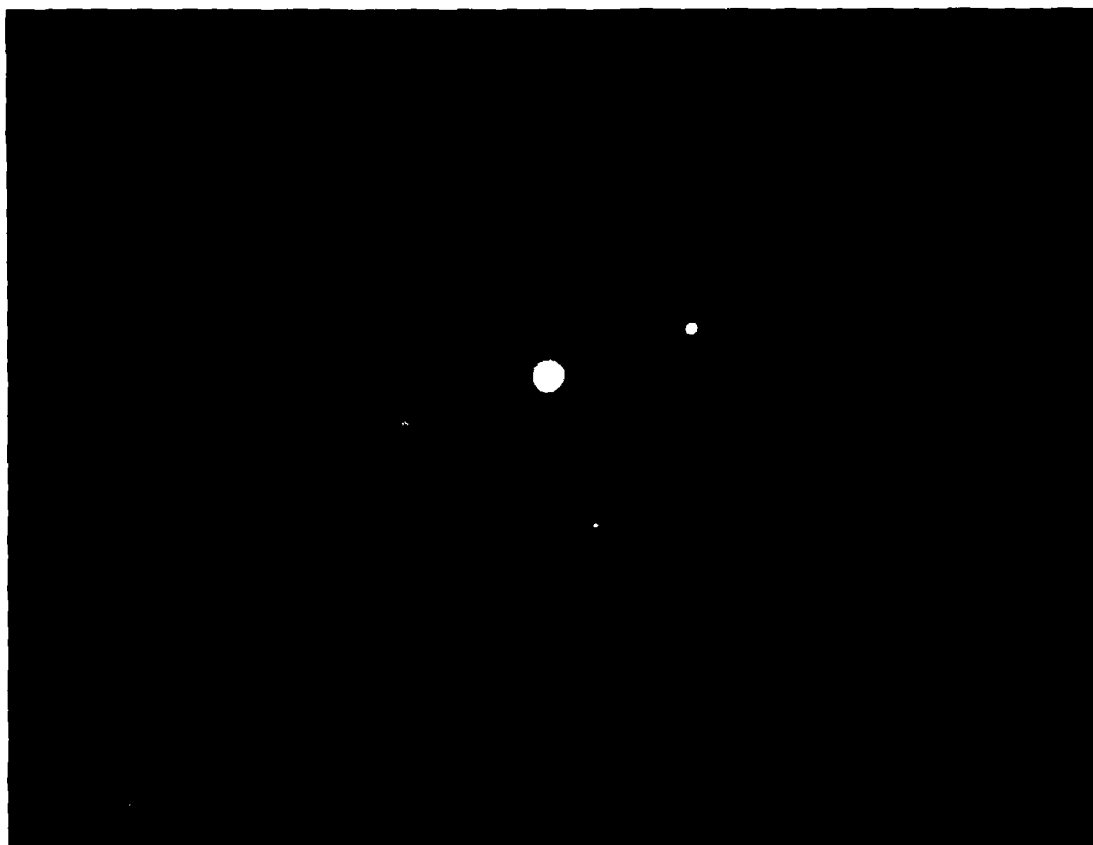


Figure 34



Figure 35



Z. A.

o Ti_2Co ($\bar{2} 0 1$)

o α ($30\bar{3}2$)

Figure 36

selected area diffraction (SAD) pattern obtained from this area of the specimen. Ti_2Co particles (arrowheads in Fig. 33) have clearly nucleated at alpha:beta boundaries and then alpha has grown round them and/or nucleated at alpha:beta or Ti_2Co :beta interfaces. Fig. 34 thus shows that a number of Ti_2Co crystals have the same spatial orientation, as is to be expected if they nucleated at an alpha:beta boundary with an essentially constant boundary orientation. This mode of bainitic compound formation is identical to that described by Hultgren (57) for the bainite reaction in carbon and alloy steels in 1947. Precipitation of alloy carbides in this manner at austenite:ferrite boundaries of high-alloy steels is currently termed interphase boundary precipitation (58) but is of course the same process. A theoretical treatment of this process, rationalizing its main features, was developed with the support of this grant and published some years ago (59). Fig. 35 shows misfit dislocations at an alpha:beta boundary. Small dark particles of Ti_2Co are seen to be associated with some of these dislocations; examples are indicated by arrowheads. This association, and especially distinction between nucleation at dislocations vs. growth ledges, remain to be sorted out during the coming report year. Analysis of the SAD pattern in Fig. 36, taken of this area, shows that the orientation relationships between alpha and Ti_2Co are: $(0001)_\alpha // (100)_{Ti_2Co}$, $[\bar{1}2\bar{1}0]_\alpha // [0\bar{1}0]_{Ti_2Co}$. The alpha phase diffraction spots are seen to be split. This is due to a slight misorientation between the lattices of eutectoid alpha and of proeutectoid alpha. Fig. 37, taken of another area,, shows the low-angle boundary between the two alphas expected but not visible in Fig. 33. This misorientation could have arisen from sympathetic nucleation of eutectoid alpha at alpha:beta boundaries; previous work, by Mr. Menon, on this program, has shown that the sympathetic nucleation process during the proeutectoid alpha reaction in a Ti-Cr alloy (and doubtless in other Ti-base alloys as well) results in a slight misorientation of the crystal thus produced with respect



Figure 37

to its substrate alpha crystal. However, from the standpoint of supersaturation, a more likely nucleation site for eutectoid alpha would be a β : Ti_2Co interfaces - or perhaps even the junction lines of alpha, β and Ti_2Co crystals. The particular boundary orientation of that portion of a Ti_2Co crystal (for example) which served as (at least part of) the substrate seems likely to influence the precise orientation relationship taken up by the eutectoid alpha crystal nucleated at this site. Clearly, though, further inquiry into this point is needed. Fig. 38 provides indications that both eutectoid alpha (Fig. 38a) and bainitic Ti_2Co grow by means of the ledge mechanism; typical growth ledges are indicated by arrowheads.

D. The Bainite Reaction in a Ti-5.2 W/O Fe Alloy

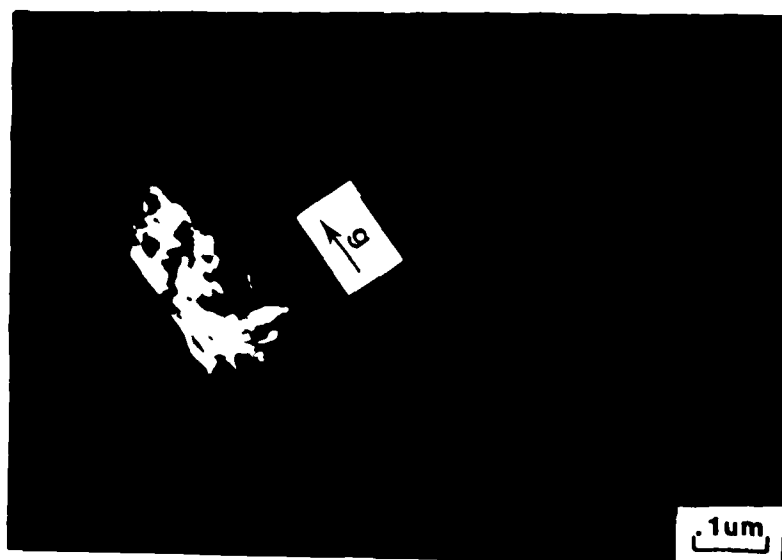
The eutectoid reaction in the Ti-Fe system is $\beta \rightarrow \alpha + \text{TiFe}$, where TiFe is CsCl-ordered bcc, $a_0 = 0.2886 \text{ nm}$. The eutectoid temperature and composition are 585 C and 14.5 W/O, respectively.

Fig. 39 shows with unusual clarity the interfacial structure at an edge of an alpha plate. Close inspection shows that dislocations in the matrix phase sometimes connect with the densely arrayed linear striations which laterally encircle this plate suggesting that they may be misfit dislocations. Fig. 40 shows a bainitic TiFe crystal clearly nucleated at a β :alpha boundary. In this situation, it appears that alpha has begun to engulf this crystal by continued growth of the right hand alpha plate. Growth ledges can be discerned on both alpha and TiFe. Spacing between growth ledges on alpha averages ca. 80 nm whereas that on TiFe is approximately 40 nm.

It is now becoming clear that, as should be expected from recent developments in nucleation theory (51) and in comparisons of nucleation theory with experiment (60), that orientation relationships which result in the predominance of partially



a



b

Figure 38



Figure 39



Figure 40

coherent interphase boundaries and thus in growth via the ledge mechanism are as ubiquitous in the bainite reaction as they are in the precipitation of a single phase from solid solution. Hackney and Shiflet (61) have recently (but earlier) reached the same conclusion about pearlite in steel, thereby upsetting "established" theory, due to Hillert (56) and C.S. Smith (62), in which the primacy of disordered interphase boundaries is considered a fundamental characteristic of this mode of eutectoid decomposition.

E. A Re-examination of the Influence of Prior Recrystallization of Proeutectoid Alpha upon the Mechanism of Eutectoid Decomposition

In 1978, Diebold, Aaronson and Franti (63) published, with the support of the present grant, a Communication presenting the results of the following experiment. Following the approach of C.S. Smith (64), specimens of a Ti-6.2 W/O Ni alloy were cold rolled to a reduction of approximately 80% in thickness (the maximum reduction that could be imposed without incurring severe cracking), reacted 5 C above the eutectoid temperature in order to recrystallize the proeutectoid alpha and dissolve intermetallic compound crystals present, and then isothermally reacted at various temperatures not far below that of the eutectoid. Despite the severe cold working imposed, the recrystallized alpha, though no longer plate shaped, still had the appearance of at least partially faceted idiomorphs. Nonetheless, at one of the sub-eutectoid temperatures used the wholly bainitic mechanism of eutectoid decomposition which characterizes hypoeutectoid Ti-Ni alloys (6) was replaced by that of pearlite. The nodules of pearlite thus produced were coarse, with rather ill-formed Ti_2Ni lamellae, but were nonetheless unmistakably of the pearlitic rather than the bainitic genre.

The Diebold et al investigation utilized only optical microscopy. Since then, however, the results of a study by Hackney and Shiflet (61) on the interfacial structures associated with pearlite in steel have become available to us. Contrary

to the Smith (62)-Hillert (56) theory, they found that the broad faces and the leading edges of ferrite and carbide lamellae are partially coherent. These results accordingly require a revision of the explanation offered, on the basis of Smith-Hillert theory, by Diebold et al for their results. This explanation posited that the recrystallized alpha:beta boundaries, being largely disordered, were able to evolve into alpha lamellae in conjunction with simultaneous precipitation of carbide lamellae. In order to provide additional information needed to revise this explanation into consistency with the Hackney-Shiflet findings, it was decided to re-examine the specimens generated by Diebold et al with TEM.

Fig. 41-43 summarize the results of this study. They are all TEM micrographs of a specimen which, after recrystallization for 7 days at 780 C, was further reacted for 4hrs. at 757 C; this processing cycle was shown by the optical microscopy studies to be capable of replacing bainite by pearlite. All three of these Figures are taken in dark-field, utilizing $(10\bar{1}0)_\alpha$, $(110)_\beta$ and $(333)_{\text{Ti}_2\text{Ni}}$ reflections, respectively. Figs. 41 and 42 show fine-scale parallel protuberances issuing from the "recrystallized" alpha:beta interface, directed toward the remaining beta matrix. Fig. 43 displays crude Ti_2Ni lamellae, some in contact with and others left well behind the advancing alpha:beta interface. Note the indications of growth ledges and perhaps also misfit dislocations at the $\alpha:\text{Ti}_2\text{Ni}$ interfaces. Taken together, this evidence indicates that: (i) the thermomechanical processing treatment used has evidently not succeeded in ensuring that recrystallized alpha:beta interfaces are disordered over their entire area, as indirectly but rather convincingly demonstrated by the evolution of parallel sideplates from these interfaces into the beta matrix; (ii) the partially coherent areas, which are immobile between ledges, were thus available at which Ti_2Ni could nucleate, in accord with theory (59); (iii) the parallelism of the Ti_2Ni plates to each other, and close inspection of Fig. 41 (where a few Ti_2Ni crystals may be discerned in between alpha sideplates), suggest that the broad

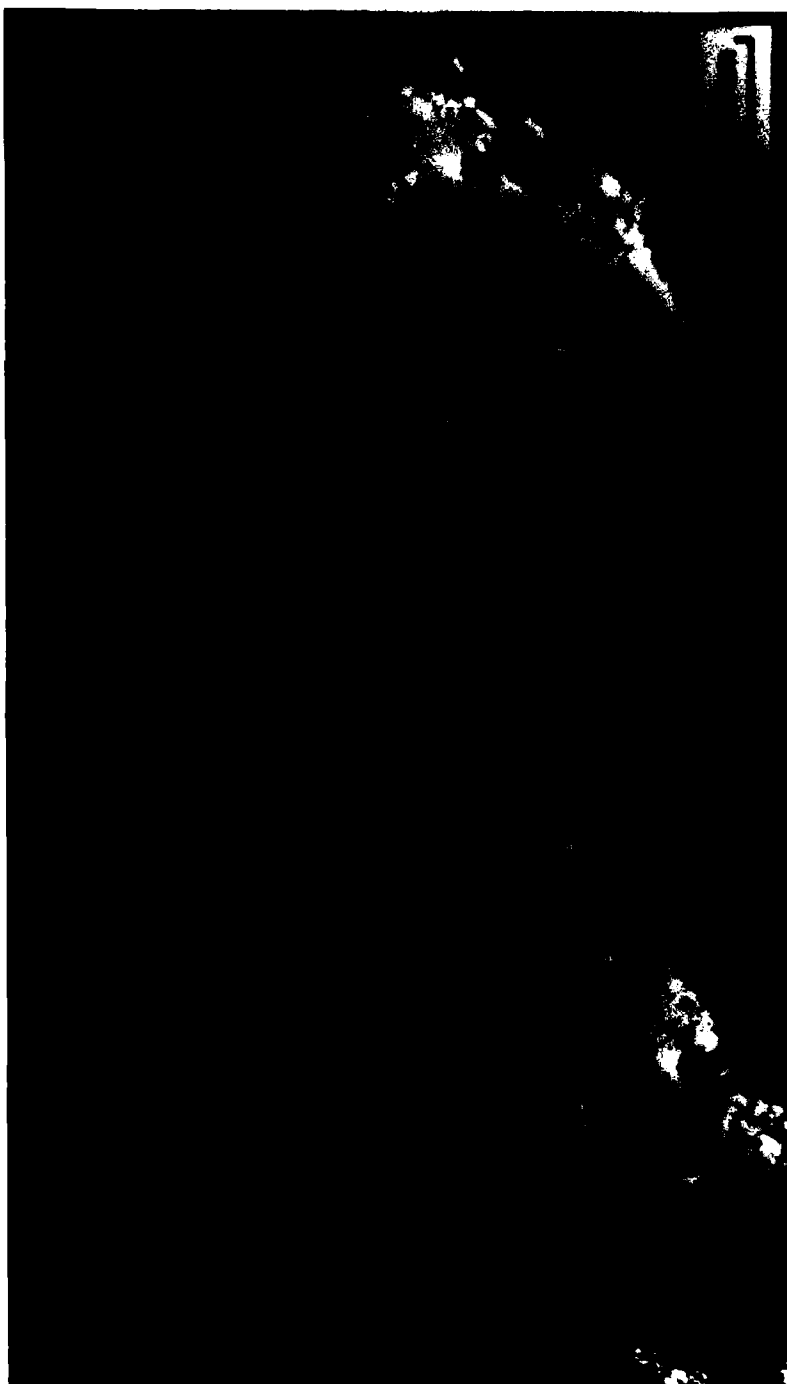


Figure 41



Figure 42

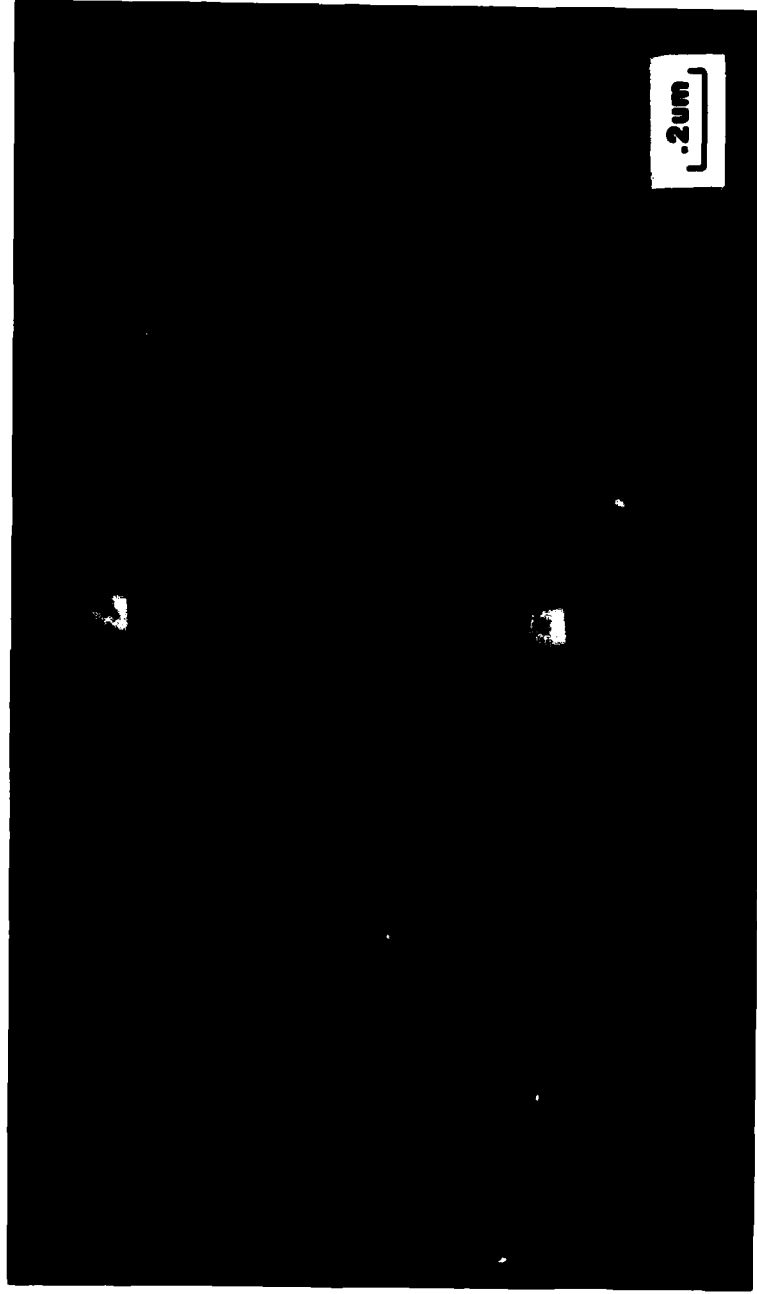


Figure 43

faces of the sideplates provide the immobile nucleation sites needed to form Ti_2Ni and (iv) the resulting microstructure is perhaps better described as bainite than as pearlite, since alpha sideplates appear to be the "leading" phase, with Ti_2Ni crystals nucleating irregularly and repeatedly behind the edges of the growing sideplates.

The following experiments remain to be performed before these conclusions can be fully accepted: (1) partial coherency should be demonstrated at least at the broad faces of the sideplates evolved from the recrystallized alpha:beta interfaces; (2) as indirect supportive evidence, the presence of near-rational orientation relationships across such interfaces ought to be sought, and (3) the precise locations of Ti_2Ni crystals relative to the sideplates must be established during an early stage in their formation.

IV. Interaction with Structural Materials Branch, Materials Laboratory, AFWAL

At the suggestion of Dr. Alan H. Rosenstein, AFOSR Program Manager, the P.I. has begun interacting with research personnel and programs at the AFWAL Materials Laboratory at Wright-Patterson Air Force Base. Through the good offices of Dr. Harris M. Burte, an introduction was arranged to Dr. F.H. Froes, Titanium Area Manager of the Structural Materials Branch. All subsequent interactions have been conducted through Dr. Froes. Within the past year, the P.I. has paid three visits to Dr. Froes' operations. During two of these visits, he gave a seminar directed, at Dr. Froes' suggestion, toward comparisons of phase transformations in titanium alloys with those in steel. This approach has, in fact, set the theme of the P.I.'s visits. Except for the seminar, these visits consist of tightly scheduled discussion sessions with individual investigators or small groups of investigators, focussed upon research programs on which they are currently working. The P.I.'s offerings during these

discussions have been based on knowledge and understanding gathered during research on phase transformations in both titanium alloys and steel. Much of this research has been sponsored by AFOSR, and earlier by the Air Force Materials Laboratory when the P.I. was a postdoctoral at Carnegie Institute of Technology (now CMU). Particularly in the case of the proeutectoid ferrite reaction in steel and the proeutectoid alpha reaction in titanium alloys, the relationships are sufficiently close to permit ready transfer of knowledge--provided that a little prudence is exercised to ensure that certain differences between these materials are not overlooked. Perhaps the best example of this transfer occurred at the outset of this series of visits, when it became apparent to the P.I. that his AFWAL colleagues had found the same effect of matrix grain size upon formation of the Widmanstatten structure in titanium alloys as had long been known in steel. As previously noted, the P. I. had attempted to determine whether or not this effect exists 25 years ago when a postdoctoral at C.I.T., but without result because of inability to refine appreciably the beta grain size of his Ti-Cr alloys. At least three different mechanisms are presently in use at AFWAL through which substantial reductions in beta grain size can be achieved, thus making possible an in-depth investigation of the effect of grain size upon the mechanics of Widmanstatten alpha formation.

The P.I. has also begun to participate in some of Dr. Froes' programs on the grain size effect and during his next visit to WPAFB will join his colleagues in preparing one or two papers for publication on the subject. The P.I. has found these visits most enjoyable, and they have usefully impacted both his research and teaching activities. He accordingly looks forward to continuing them for as long as he can be useful to AFWAL staff.

References

1. H. I. Aaronson, "The Mechanism of Phase Transformations in Crystalline Solids", p. 270, Institute of Metals, London (1969).
2. M. Hillert, Jernkontorets Annaler, 141, 757 (1957).
3. M. R. Plichta, J. C. Williams and H. I. Aaronson, Met. Trans. 8A, 1885 (1977).
4. M. R. Plichta, unpublished research, University of Utah, 1983.
5. H. I. Aaronson, W. B. Triplett and G. M. Andes, Trans. AIME, 209, 1227 (1957).
6. G. W. Franti, J. C. Williams and H. I. Aaronson, Met. Trans. 9A, 1641 (1978).
7. E.S.K. Menon, M.R. Plichta and H. I. Aaronson, Scripta Met., 17, 1455 (1983).
8. J.L. Murray, Bull. Alloy Phase Diagrams, 3, 94 (1982).
9. J.L. Murray and K.J. Bhansali, Bull. Alloy Phase Diagrams, 4, 178 (1983).
10. M.R. Plichta, H.I. Aaronson and J.H. Perepezko, Acta Met., 26, 1293 (1978).
11. J.W. Christian, "The Theory of Phase Transformations in Metals and Alloys", Ch. XI, Pergamon Press, Oxford (1965).
12. A.M. Brown and M.F. Ashby, Acta. Met., 28, 1085 (1980).
13. G. Horvay and J.W. Cahn, Acta Met., 9 695 (1961).
14. E.S.K. Menon, R.W. Hyland and H.I. Aaronson, Scripta Met., 18, 367 (1984).
15. J. Askill and G.B. Gibbs, Phys. Stat. Sol., 11, 557 (1965).
16. J. Askill, Phys. Stat. Sol., 43b, K1 (1971).
17. J.W. Cahn, Acta Met., 4, 449 (1956).

18. T. Obara, W.F. Lange III, H.I. Aaronson and B.E. Dom, "Proceedings of an International Conference on Solid-Solid Phase Transformations", p. 1105, TMS-AIME, Warrendale, PA (1983).
19. T. Sato, S. Hukai and Y.C. Huang, Jnl. Austral. Inst. of Met., 5 (2), 149 (1960).
20. C.G. Rhodes and J.C. Williams, Met. Trans., 6A 2103 (1975)
21. G. Hahn, Senior Thesis, NYU, quoted in P.A. Albert, TMS-AIME, 197 1449 (1953).
22. P.D. Frost, W.M. Parris, L.L. Hirsch, J.R. Doig and C.M. Schwartz, Trans. ASM, 46, 231 (1954).
23. M.J. Pool, R. Speiser and G.R. St. Pierre, TMS-AIME, 239 1180 (1967).
24. M.K. Koul and J.F. Breedis, Acta Metall., 18 579 (1970).
25. J.L. Murray, Bull. Alloy Phase Diagrams, 2 185 (1981).
26. G. Hari Narayanan, T.S. Luhman, T.F. Archbold, R. Taggart and D.H. Polonis, Metallography, 4 343 (1971)
27. V. Chndrasekharan, R. Taggart and D.H. Polonis, Metallography, 5 393 (1972).
28. E.S.K. Menon, S. Banerjee and R. Krishnan, Trans. Ind. Inst. of Met., 31 305 (1978).
29. J.L. Murray, Bull. of Alloy Phase Dia., 2 174 (1981).
30. J.W. Cahn, J. Am. Ceram. Soc., 52 118 (1969)
31. E.S.K. Menon, S. Banerjee and R. Krishnan, Met. Trans., 9A 1213 (1978).
32. P.E.J. Flewitt, Acta Met., 22 47 (1974).
33. Idem, ibid, 22 65 (1974).
34. G.K. Dey and S. Banerjee, J. Nucl. Matls., 125, 219 (1984).
35. P. Mukhopadhyay, E.S.K. Menon, S. Banerjee and R. Krishnan, Zeit. Metalkde, 69 725 (1978).
36. H.I. Aaronson, unpublished research, Carnegie Institute of Technology, (1957).

37. S. Krishnamurthy, R. G. Vogt, D. Eylon and F. H. Froes, Proc. 1983 Annual Powder Metallurgy Conference, American Powder Metallurgy Institute.
38. P. R. Krahe, K. R. Kinsman and H. I. Aaronson, Acta Met., 20 1109 (1972).
39. C.M. Wayman, "Phase Transformations", p. 59, ASM, Metals Park, OH (1970).
40. K.R. Kinsman, E. Eichen and H.I. Aaronson, Met. Trans., 6A, 303 (1975).
41. J.D. Watson and P.G. McDougall, Acta Met., 21, 961 (1973).
42. H.M. Clark and C.M. Wayman, Met. Trans., 3, 1979 (1972).
43. C.M. Wayman and G.R. Srinivasan, "The Mechanism of Phase Transformations in Crystalline Solids", p. 310, Institute of Metals, London (1969).
44. K.R. Kinsman, R.H. Richman and J. Verhoeven, "National Science Symposium Abstracts", p. 41, ASM, Metals Park, OH (1974).
45. H.K.D.H. Bhadeshia, Acta Met., 29, 1117 (1981).
46. H.I. Aaronson, G.J. Shiflet, S.K. Liu, W.T. Reynolds, Jr. and D.A. Smith, Met. Trans., in press.
47. J.W. Christian, "Decomposition of Austenite by Diffusional Processes", p. 371, Interscience, NY (1962).
48. S.K. Sikka, K.Y. Vohra and R. Chidambaram, Prog. Mat. Sci., 29, 245 (1982).
49. H.I. Aaronson, Trans. TMS-AIME, 224, 693 (1962).
50. H.I. Aaronson, W.B. Triplett and G.M. Andes, Trans. TMS-AIME, 218, 331 (1960).
51. H.I. Aaronson and K.C. Russell, Proceedings of an International Conference on Solid-Solid Phase Transformations, p. 371, TMS-AIME, Warrendale, PA (1983).
52. R.A. Ricks and P.R. Howell, Acta Met., 31, 853 (1983).
53. M.R. Plichta and H.I. Aaronson, Acta Met., 28, 1041 (1980).
54. P.L. Ryder, W. Pitsch and R.F. Mehl, Acta Met., 15, 1431 (1967).

55. A. D. King and T. Bell, Met. Trans., 7A, 1419 (1975).
56. M. Hillert, "Decomposition of Austenite by Diffusional Processes", p. 241, Interscience, NY (1962).
57. A. Hultgren, Trans. ASM, 39, 915 (1947).
58. R.W.K. Honeycombe, Met. Trans., 7A, 915 (1976).
59. H.I. Aaronson, M.R. Plichta, G.W. Franti and K.C. Russell, Met. Trans., 9A, 1339 (1978).
60. M.R. Plichta, J.H. Perpezko, H.I. Aaronson, and W.F. Lange III, Acta Met., 28, 1031 (1980).
61. S.A. Hackney and G.J. Shiflet, in preparation for Acta Met. (Univ. of Virginia).
62. C.S. Smith, Trans. ASM, 45, 533 (1953).
63. T.P. Diebold, H.I. Aaronson and G.W. Franti, Met. Trans., 9A, 1339 (1978)
64. C.S. Smith, Trans. AIME, 175, 15 (1948).

LIST OF FIGURE CAPTIONS FOR MICROGRAPHS

- Figure 11: a) Surface reliefs of proeutectoid α plates in Ti-7.15 W/O Cr reacted at 687°C for 70 min. b) Interference micrograph of the same area (xenon illumination; $\lambda = 0.546 \mu\text{m}$).
- Figure 12: a) Bright field TEM micrograph of proeutectoid α plates Ti-7.15 W/O Cr reacted at 687°C for 70 min. b) Dark field micrograph of the same area using an α phase reflection.
- Figure 13: SAD pattern of the same area as Fig. 12; the indexed pattern shows Burgers orientation relationship between α and β . Extra spots derive from the ω phase.
- Figure 14: Other types of bainite nodules in Ti-25 W/O Cr reacted at 665°C. a) Formation of sideplate bainite nodules after one hr. of reaction. b) Competition between hemispherical bainite nodules and sideplate nodules, following reaction for 4 hrs. c) Band or sheet type of bainite structure, resulting from impingement of sideplate and hemispherical bainite nodules; reacted 90 min. and etched in 60% glycerine, 20% HNO_3 , 20% HF.
- Figure 15: Overall view of bainite nodule formation along grain boundaries in Ti-25 W/O Cr; reacted at 665°C for 90 min. Note variations in nodule morphology at the different grain boundaries. Etched in 60% glycerine, 20% HF, 20% HNO_3 .
- Figure 16: Formation of bainite nodules at proeutectoid intragranular TiCr_2 plates in Ti-25 W/O Cr reacted at 665°C for 5 hrs. Etched in 60% glycerine, 20% HF, 20% HNO_3 .
- Figure 17: SEM micrograph of Ti-25% Cr reacted 1 hr. at 665°C, showing sideplate nodules (above grain boundary) and spherical nodules (below) of bainite. Dark minority phase TiCr_2 , light phase is eutectoid α and black background is retained beta.
- Figure 18: SEM micrograph of same specimen as in Fig. 17, illustrating intragranularly nucleated bainite nodules.
- Figure 19: TEM micrograph of Ti-25 W/O Cr reacted 90 min. at 665°C, showing internal structure of bainite nodule.
- Figure 20: Dark field micrograph of same area as Fig. 19, taken with $(10\bar{1}0)_\alpha$ reflection, illustrating misfit dislocations at interphase boundaries.
- Figure 21: Higher magnification view of a portion of the area in Fig. 20, taken in dark field with $(110)_\beta$ reflection, illustrating more clearly pronounced facets on beta: TiCr_2 interface.
- Figure 22: Bright field micrograph of Ti-25% Cr specimen reacted 90 min. at 665°C, illustrating interfacial structure within sideplate bainite nodule.
- Figure 23: Dark field micrograph using an α phase reflection in Ti-25 W/O Cr, reacted at 665°C for 90 min.
- Figure 24: Bright field micrograph of Ti-25 W/O Cr reacted at 665°C for 90 min. showing a facet region within a curved interface.

- Figure 25: a) Bright field micrograph in Ti-25 W/O Cr reacted at 665°C for 90 min.
b) Dark field micrograph of the same area taken with an α reflection.
- Figure 26: Bright field micrograph of Ti-25 W/O Cr reacted at 665°C for 90 min. TiCr_2 appears to have formed at a planar beta:bainitic alpha boundary.
- Figure 27: Dark field micrographs of the same area seen in Fig. 25, using TiCr_2 reflections. a) and b) show differences in the orientations of TiCr_2 crystals within the same bainitic nodule.
- Figure 28: Bright field micrograph in Ti-25 W/O Cr reacted at 665°C for 90 min., illustrating a TiCr_2 crystal protruding in front of a bainite nodule.
- Figure 29: Growth kinetics of hemispherical bainite nodules in Ti-25 W/O Cr at 665°C.
- Figure 30: Dark field micrograph of Ti-3.9 W/O Co reacted for 40 min. at 625°C taken from $(110)_\beta$ reflection. Misfit dislocations are regularly spaced and seen as thin, parallel lines; meanwhile growth ledges are more irregularly spaced (thicker black lines). Also superledges consisting of several growth ledges are seen on lower α plate.
- Figure 31: Dark field micrograph of the adjacent area in Fig. 30, illustrating more than one array of misfit dislocations and closely spaced growth ledges on superledges.
- Figure 32: Dark field micrograph of Ti-3.9 W/O Co reacted for 40 min. at 625°C taken with $(110)_\beta$ reflection. Misfit dislocations and growth ledges are seen at the edges of alpha plate.
- Figure 33: Bright field micrograph of Ti-3.9 W/O Co reacted at 625°C for 40 min., showing the intermetallic compound Ti_2Co nucleated at alpha:beta interfaces and further growth of alpha phase leaving intermetallic compound behind as arrows indicated.
- Figure 34: Dark field micrograph of the same area in Fig. 33 taken from $(020)_{\text{Ti}_2\text{Co}}$ reflection, showing that a number of Ti_2Co have the same spatial orientation.
- Figure 35: Dark field micrograph of the same area in Fig. 33 taken from $(200)_\beta$ reflection, showing the misfit dislocations and intermetallic compounds associated with them as dark particles.
- Figure 36: SAD pattern of the same area in Fig. 33 and indexed pattern, showing $(0001)_\alpha // (100)_{\text{Ti}_2\text{Co}}$, $[\bar{1}2\bar{1}0]_\alpha // [0\bar{1}0]_{\text{Ti}_2\text{Co}}$ orientation relationship. Spots of alpha phase are split due to the misorientation between the lattices of eutectoid alpha and proeutectoid alpha.
- Figure 38: a) Bright field micrograph of Ti-3.9 W/O Co reacted at 625°C for 40 min., showing the growth of both eutectoid alpha and Ti_2Co by ledge mechanisms.
b) Dark field micrograph of the same area, showing the growth ledges on Ti_2Co phase.
- Figure 39: Bright field micrograph of Ti-5.2 W/O Fe reacted at 550°C for 154 days, showing the edge of alpha plates consisting of misfit dislocations.

Figure 40: Bright field micrograph of Ti-5.2 W/O Fe reacted at 550°C for 154 days, showing the intermetallic compound TiFe at the alpha:beta interfaces. Both TiFe and eutectoid alpha grow by ledge mechanisms.

Figure 41: Dark field micrograph of Ti-5.1 a/o Ni recrystallized at 780°C for 7 days after cold rolling and isothermally heat-treated at 757°C for 4 hours taken from $(10\bar{1}0)_\alpha$ reflection, illustrating the fine-scaled protuberances at the alpha:beta^α interface.

Figure 42: Dark field micrograph of the same specimen in Fig. 41 taken from $(110)_\beta$ reflection, showing protuberances of alpha phase at alpha:beta interfaces.

Figure 43: Dark field micrograph of the same specimen in Fig. 41 taken from $(333)_{Ti_2Ni}$ reflection, illustrating the crude Ti_2Ni lamellae with dislocation boundaries at alpha: Ti_2Ni interface.

END

FILMED

6-85

DTIC